The University of Kansas

Technical Report

Receiver Antenna Array for a Multichannel Sense-and-Avoid Radar for Small UAVs

Jose Francisco Florencio Neto

ITTC-FY2013-TR-70093-01

April 2013

Project Sponsor:
NASA
Stennis Space Center

Abstract

A receiver monopole antenna array is designed for use in a sense-and-avoid radar for use in the Cessna C-172 and small Unmanned Aerial Vehicles (UAVs). This three element array is used for range, radial velocity and azimuthal angle calculations. After modeling and simulating it, the array is designed, implemented and finally tested in an anechoic chamber. These results are compared to both simulation and theoretical results. Since this array was designed to face harsh weather conditions, a protective dome made with ABS plastic is designed to cover it. The simulated effects of this dome on the array's radiation pattern are analyzed and compared to the array's pattern without the dome.

This fabricated array has a center frequency of 1.4454 GHz and has good reflection coefficient and coupling levels over the range of frequencies tested (1.35 to 1.5 GHz). The maximum gain of its elements varies between 0 and 2.2 dBi for this frequency range.

Table of Contents

List of Figures

Chapter 1: Introduction

1.1 Project Motivation

1.1.1 Multichannel Sense-and-Avoid Radar for UAVs

The use of UAVs today is an area that is far from being fully explored. Primarily used for military purposes, but also for civil applications such as firefighting, policing, and general security application, UAVs offer the chance to perform various tasks without putting human lives in immediate danger. Using Remote Control (RC), UAVs can oversee large areas as long as it is within eyesight of its controller. Once it falls out of sight, different problems occur such as the possibility of other moving airborne objects hitting it or a collision with power towers, lines, skyscrapers, and other non-moving objects. From this fact, comes the main motivation for this project. With a reliable way to sense and avoid these obstacles, the range of applications for UAVs is dramatically increased as they become more independent of the controller and can, therefore, reach areas that were once unreachable. After an obstacle is detected, the data are processed, and ultimately sent to the UAVs auto-pilot, which takes care of the avoidance of the obstacle. This represents a tremendous advance when compared with the relatively short distance applications that are currently in place.

1.1.2 Multiple Antennas to Account for Multiple Measurements

The motivation to use a Multichannel Radar in this project comes from the fact that various measurements need to be taken to correctly sense and avoid incoming obstacles. The first and most important required measurement is range. Once an approaching object reaches a range of 1 Nautical Mile (1852 m) to the UAV, the Radar needs to be able to detect its presence. The

second measurement taken is radial velocity. The motivation behind the need to take this measurement is that it is necessary to know how fast the approaching object is coming towards the UAV, since not all the detected objects will be stationary. The third and fourth required measurements are elevation and azimuth angles. These two measurements together with range give the exact 3-D location of the approaching object. The need for these four measurements determines the amount of receiver channels needed: a minimum of four. As will be explained further, for a greater ease in the antenna array manufacturing process, five receiving channels will be used in this project.

1.2 Background of Antenna Theory

1.2.1 S Parameters

Scattering parameters (or S parameters) can be used to represent the port characteristics of RF circuits. The number of S parameters depends on how many ports the circuit has. An n-port circuit has an n x n S parameter matrix:

$$\begin{bmatrix} s_{11} & \cdots & s_{1n} \\ \vdots & \ddots & \vdots \\ s_{n1} & \cdots & s_{nn} \end{bmatrix}$$

From this matrix, each S parameter can be expressed in terms of the ratio of an outgoing and incoming voltage phasor [1].

$$s_{11} = \frac{V_1^-}{V_1^+} \; when\ all\ other\ ports\ are\ matched \qquad (1.1)$$

$$s_{1n} = \frac{V_1^-}{V_n^+} \; when\ port\ 1\ is\ matched \qquad (1.2)$$

$$s_{n1} = \frac{V_n^-}{V_1^+} \; when \; port \; n \; is \; matched \tag{1.3}$$

$$s_{nn} = \frac{V_n^-}{V_n^+} \; when \; all \; other \; ports \; are \; matched \tag{1.4}$$

The terms in the main diagonal of the S matrix represent the reflection coefficients (Γ) of each port [2].

$$\Gamma = \frac{V^-}{V^+}\Big| z = 0 \tag{1.5}$$

All other terms in the S matrix represent the coupling waves from one port to the other. For reciprocal networks, the s_{mn} terms are equal to the s_{nm} terms (where m is not equal to n) [1].

Other properties can also be obtained from the s_{mn} and s_{nm} parameters. These include the complex linear gain, scalar linear gain and scalar logarithmic gain [3].

Complex linear gain:

$$G = s_{mn} \tag{1.6}$$

Scalar linear gain:

$$|G| = |s_{21}| \tag{1.7}$$

Scalar logarithmic gain:

$$g = 20log_{10}|s_{21}| \; dB \tag{1.8}$$

1.2.2 Z Parameters

The Impedance parameters (or Z parameters) of a network are directly related to its S

parameters. The relationship between the port currents, port voltages and the Z-parameter matrix [4] is given by

$$\begin{bmatrix} V_1 \\ \vdots \\ V_n \end{bmatrix} = \begin{bmatrix} Z_{11} & \cdots & Z_{1n} \\ \vdots & \ddots & \vdots \\ Z_{n1} & \cdots & Z_{nn} \end{bmatrix} \begin{bmatrix} I_1 \\ \vdots \\ I_n \end{bmatrix} \tag{1.9}$$

where

$$Z_{mn} = \frac{V_m}{I_n}\Big| I_k = 0 \; for \; k \neq m \; [\Omega]$$

The Z parameters in the main diagonal of the matrix above are the input impedances of port N when all other ports in the network are open circuited [5].

One can determine the Z parameters from the S parameters using the following relationships:

$$[\boldsymbol{Z}] = -Z_O[[\boldsymbol{S}] - [\boldsymbol{I}]]^{-\mathbf{1}}\big[[\boldsymbol{S}] + [\boldsymbol{I}]\big][\boldsymbol{\Omega}] \tag{1.10}$$

where **I** is the identity matrix.

There are at least three reasons why it might be desirable to use S parameters instead of Z parameters at high frequencies:

(1) Measuring the Z parameters of a network requires open circuits at the ports. Many devices will have parasitic oscillations when a port is open circuited. This does not happen as often when matched loads are used.

(2) It is easier to measure traveling voltage waves than total voltages. Therefore, the S parameters have a more natural representation at higher frequencies.

(3) S matrices have mathematical properties that make them easier to work with [6].

1.2.3 Gain and Radiation Pattern

Power gain ($G_g(\theta,\Phi)$) is defined as [7]:

$$G_g(\theta,\Phi) = \frac{4\pi U(\theta,\Phi)}{P_{in}} \qquad (1.11)$$

where $U(\theta,\Phi)$ is the antenna's radiation intensity and P_{in} is the input power of a lossless reference antenna (usually an isotropic radiator) equal to:

$$P_{in} = 4\pi U_{ref}\ [W] \qquad (1.12)$$

The maximum power gain of an antenna is simply its gain in the direction where U is maximized. An antenna's 3-D radiation pattern is formed by determining its gain over all azimuth angles ($0 < \Phi < 2\pi$) and all elevation angles ($0 < \theta < \pi$). For a 2D radiation pattern, one of the two angles (Φ or θ) is held constant while the other one varies.

1.2.4 Monopoles

Dipole and monopole antennas share many similarities. First, they are both vertically polarized. Second, their radiation pattern in the azimuth plane is symmetric and identical in shape over 360º. Third, their radiation pattern in the elevation plane where $z > 0$ (above the ground plane) is also identical. Finally, their bandwidth is ~ 10% of their center frequency.

Still, there are also differences between the two that would determine the choice of one over the other. First, dipoles are usually twice as long as monopoles. While dipoles are usually a half wavelength ($\lambda/2$ or, more precisely, 0.475λ) long, monopoles are a quarter wavelength ($\lambda/4$) long with a conducting ground plane, which essentially replaces the other half of the dipole and makes their radiation pattern above the ground plane identical. This concept can be better

visualized in Figure 1.1.

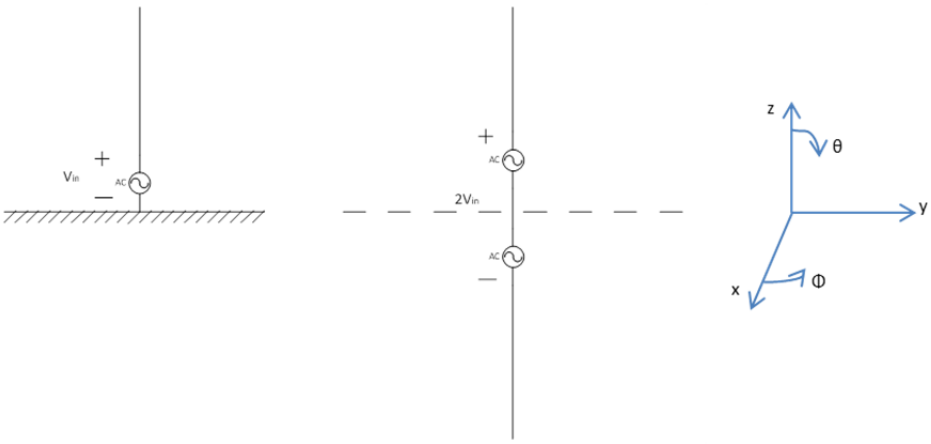

Fig. 1.1: Comparison between a monopole and a dipole.

The second main difference between dipoles and monopoles is that the radiation pattern of a monopole under the ground plane ($z < 0$) is severely attenuated. If the ground plane was infinite and ideal, the radiation pattern below the ground plane would be zero, but in the real world, perfect ground planes are impossible to be achieved, so there will still be some radiation. Third, the maximum gain of these two types of antenna are also different. For dipoles, 2 dBi at the $z = 0$ plane is typically the maximum gain. For monopoles, the typical maximum gain ranges from 2 to 6 dBi slightly above the $z = 0$ plane. Finally, the input impedance of half wavelength dipoles is $Z_{in} \approx 73 + j0\ \Omega$ while the input impedance of a quarter wavelength monopole is half of that, or $Z_{in} \approx 36.5 + j0\ \Omega$ [8].

1.3 Background of Radar Theory

1.3.1 Range and Range Resolution Determination

Continuous wave (CW) radars use a technique called frequency-modulation (FM) ranging to determine a target's range. In this technique, the frequency of the transmitted wave is varied

linearly and the range is determined by first finding the lag in time between the transmitted signal and the received echo [9]. This can be better visualized in Figure 1.2.

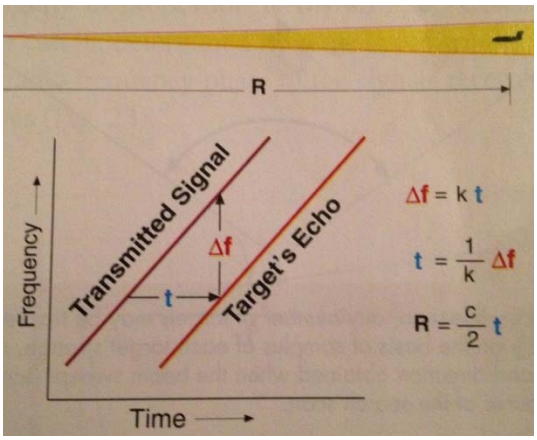

Fig. 1.2: Frequency Modulation concept used to determine range.

where Δf is also known as the beat frequency and k is the wavenumber (k = 2 π/λ).

To summarize, the range R is given by Equation 1.13:

$$R = \frac{c}{2} t \; [m] \tag{1.13}$$

where t is time.

Range Resolution (ΔR) in FMCW radars is related to the bandwidth, as shown in Equation 1.14:

$$\Delta R = \frac{c}{2B} \; [m] \tag{1.14}$$

where c is the speed of light and B is the bandwidth [10].

1.3.2 Radial Velocity Determination

Radial velocity in FMCW radars is measured using the concept of Doppler shift. The relative motion between the radar's antenna and its target is what creates this Doppler shift in the

received signal frequency. After determining range, the phase of the backscattered wave relative to its phase is

$$\Phi = -2kR = -2\pi\frac{2R}{\lambda}\ [rad] \tag{1.15}$$

where k is the wavenumber and λ is the wavelength.

Since the Doppler frequency shift is the derivative of phase with respect to time and the derivative of range with respect to time is equal to the radial velocity, the following relationship is achieved

$$f_D = -\frac{2v_r}{\lambda}\ [Hz] \tag{1.16}$$

where v_r is the radial velocity (m/s) and a negative v_r means a decreasing range and a positive v_r means an increasing range.

Finally, the radial velocity vector $\mathbf{v_r}$ can be determined if the position, **P**, and the relative velocity, **v**, of both the radar and the target are known. Using Figure 1.3

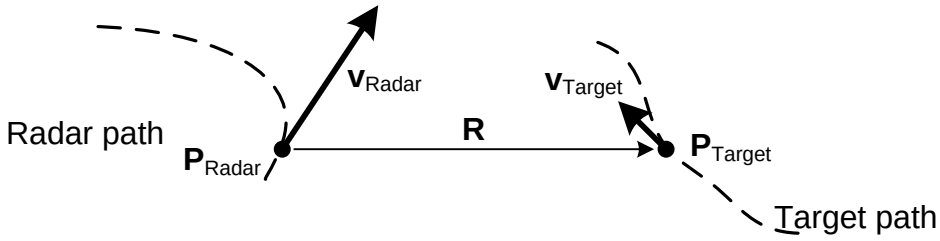

Fig. 1.3: Instantaneous path and velocity of a radar and a target.

and Equation 1.17 for **v,**

$$\boldsymbol{v} = \boldsymbol{v}_{radar} - \boldsymbol{v}_{target}\ [m/s] \tag{1.17}$$

the radial velocity is simply the dot product of the range vector, **R**, and **v**, or

$$\boldsymbol{v}_r = \vec{\boldsymbol{v}} \cdot \hat{\boldsymbol{R}}\ [m/s] \tag{1.18}$$

where $\widehat{\boldsymbol{R}}$ is the unit vector [11].

1.3.3 Azimuth Angle-of-Arrival (AoA) Determination

When a transmitted wave hits a target, is reflected, and eventually reaches the receiver antennas, the reflected wave arrives at each element of the array with a specific phase (Ψ). Using the difference in phase (δ) between two elements in the array that are in the same horizontal plane, the azimuth AoA ($\theta_{azimuth}$) can be determined using Equation 1.19:

$$\theta_{AB} = cos^{-1}\left(\frac{\lambda\delta_{AB}}{2\pi d}\right)[rad] \qquad (1.19)$$

where d is the baseline between the two elements in the array.

Having an array of at least three elements yields two arrival angles, which eliminate any ambiguity that is created by the fact that, on a given plane at a certain range, an arrival angle yields two possible target locations. This concept is shown in Figure 1.4 [12].

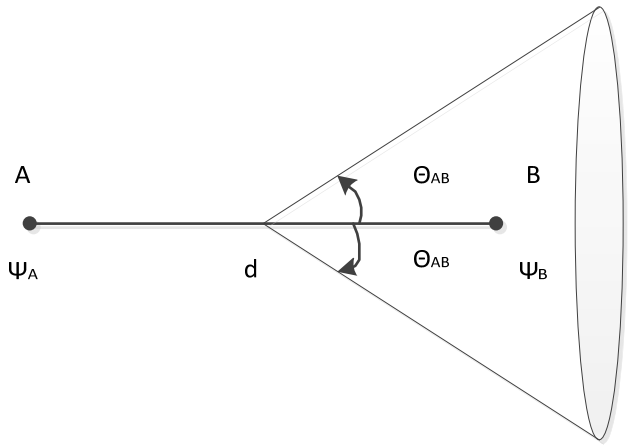

Fig. 1.4: AoA ambiguity created by a phase difference.

1.3.4 Elevation AoA Determination

Determination of the elevation AoA ($\theta_{elevation}$) is very similar to the determination of the azimuth AoA. The concept is the same, except that there is a problem with the three elements in the array lying in the same plane, as far as reaching a non-ambiguous elevation angle: there is still an ambiguity in the out-of-plane angle. This is shown in Figure 1.5.

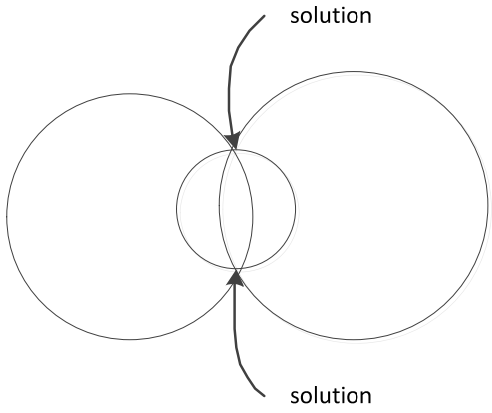

Fig. 1.5: Three equi-range paths formed by three elements on the same plane.

To eliminate this ambiguity, a fourth element is needed in a plane different than the plane of the other three elements. In other words, the fourth element needs a height offset from the other three elements. This extra step eliminates all ambiguities in $\theta_{elevation}$ [12].

1.4 Requirements and Challenges

1.4.1 +/- 15° Elevation Coverage

The chosen receiver antennas need to cover at least 30 degrees (+/- 15° from the horizon) in the elevation plane. This ensures that an object approaching the radar from this elevation angle range gets detected by the receiver antennas. It also means that the chosen antenna for elevation

angle measurement needs to have a good gain for at least this range of angles. This can be a challenge depending on what antenna type is chosen.

1.4.2 ~360° Azimuthal Coverage

The chosen receiver antennas need to have an azimuthally symmetric coverage over 360°. This means that some more directional antennas that do not satisfy this condition can be ruled out. Also, this requirement ensures that an object approaching the radar from any azimuthal direction will be properly detected.

1.4.3 ~3° Azimuthal AoA Resolution

In order to perform an accurate phase comparison between two elements so that $\theta_{azimuth}$ can be correctly calculated, the phase of each element needs to be measured at least every 3°. This means that, when calculating the phase over the 360° around an element in the anechoic chamber, at least 120 measurements for each element need to be taken.

1.4.4 1/125 NM Range Resolution

This radar's ΔR needs to be smaller than 1/125 NM. In meters, this is equivalent to a ΔR of 14.816 m. Using Equation 1.14 for ΔR in section 1.3.1, it is possible to determine the antenna bandwidth (B) that is required for this ΔR. After substituting the required ΔR into the equation, a bandwidth requirement of at least 10.1 MHz is achieved.

2.1 Overview

From the theory exposed in Chapter I, it is possible to determine the requirements for the three element receiver antenna array. These requirements also apply for the element(s) responsible for the elevation AoA measurements. All the elements need to have a good maximum gain, be azimuthally symmetric, have an element spacing of no more than λ/2 and have a frequency range that covers 1.4454 +/- .005 GHz. With these requirements in mind, three different antenna types were considered and will be further analyzed: scanning antennas, dipole antennas and monopole antennas.

2.2 Antenna Selection

2.2.1 Scanning Antennas

There are two types of scanning antennas: mechanically steered scanning antennas and electronically steered array antennas (ESAs). ESAs are mounted in a fixed position in the radar and have their beams steered by controlling the phase of the waves transmitted and received by each radiating element [13]. Both were considered for this project since they satisfy all the four main requirements expresses in section A of this chapter. Their maximum gain could even be greater than the other less complex antenna type options depending on what antenna type was chosen for this scanning antenna array. For example, if parabolic antennas were chosen in a mechanically steered antenna array, their maximum gain could potentially be 25 dB greater than a monopole's maximum gain, and 28 dB greater than a dipole's maximum gain [14]. The problems with choosing a scanning antenna array are that not only they increase the complexity

of the system, giving it a higher probability for errors, but they are also much more expensive than dipoles or monopoles. Also, scanning arrays will probably have a greater weight than dipole or monopole arrays, and in aviation that is a big consideration. For these three reasons, a scanning array was rejected.

2.2.2 Dipoles

The next antenna type considered for the receiver array was the half wavelength dipole. They are very simple, non-expensive antennas that also satisfy all the requirements in section A of this chapter. Their maximum gain (nominally 2.15 dBi) is obviously not as good as what it would be if a scanning antenna array was used [15]. A second problem is that, at the center frequency used in this project (1.4454 GHz), a wavelength is ~ 20 cm. This could pose problems since the half wavelength dipoles would need to be placed on the plane with a vertical orientation and it is not the best aerodynamic option to have a structure longer than 10 cm coming out of the UAV. Therefore, a different option that improves these two requirements must be searched.

2.2.3 Monopoles

A quarter wavelength monopole array was determined to be the best option for this project. It satisfies the four requirements from section A of this chapter and offers two very important improvements from the dipole option. First, the maximum gain of a monopole is 3dB over the maximum gain of a half wavelength dipole (nominally 5.15 dBi) [16]. Second, the length of a monopole is half as long as the length of a dipole. Since the center frequency used is 1.4453 GHz, the wavelength is 20.75 cm. This would make the half wavelength dipoles (actually 0.475λ dipoles) to be 9.86 cm and a quarter wavelength dipole to be half of that, or 4.93 cm. The

downside of this option is that the monopole array needs a ground plane with a radius of at least λ/4. The bigger the ground plane, the better the array's radiation pattern, so a ground plane with a radius of 11.22 cm was chosen [17].

2.3 Modeling and Simulation

2.3.1 Overview

A monopole array using 4.9-cm long monopoles and an 11.22-cm radius ground plane was modeled and simulated in ANSYS' software HFSS™. Lumped ports were used as the monopole feeds, copper was chosen as both the monopole and ground plane material, and the whole array was placed in a radiation box. The separation between the monopoles and the ground plane was set to 1.34 mm of FR-4 material and the thickness of the monopoles was set to 0.034 mm (these dimensions are chosen according to the FR-4 sheets available in the University of Kansas' EECS Shop). The final model with the three monopoles numbered is shown in Figure 2.1.

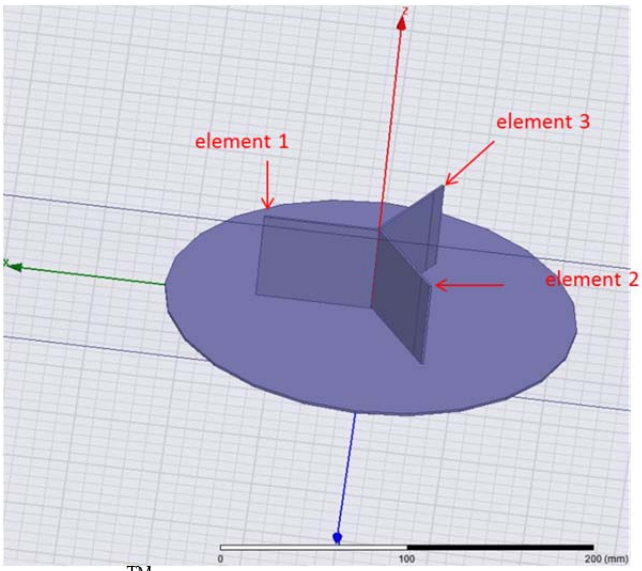

Fig. 2.1: HFSS™ model of three-element array with numbered elements.

2.3.2 Expected Results

As mentioned in section B of this chapter, the maximum gain of each monopole element should be 5.15 dBi at an elevation angle slightly less than $\theta = \pi/2$. The actual maximum gain is going to be a little less than this theoretical value of 5.15 dBi due to system losses and inaccuracies. The radiation pattern should also be azimuthally symmetric and have a significant decay at $\theta > \pi/2$. The reflection coefficient of all three elements should have a matching s_{11}, s_{22} and s_{33} vs frequency curve and the lowest value at the system's center frequency. The coupling of all three elements should also have a matching s_{12}, s_{21}, s_{13}, s_{31}, s_{23} and s_{32} vs. frequency curve and a low value (less than –10 dB) at the system's center frequency. The coupling should still be low for a frequency range of at least 10% of the center frequency, since that is the bandwidth of a quarter wavelength monopole [14].

2.3.3 Z Parameter Results

The first result extracted from the model's simulation was its impedance matrix at 1.44 GHz. This matrix is shown in Figure 2.2.

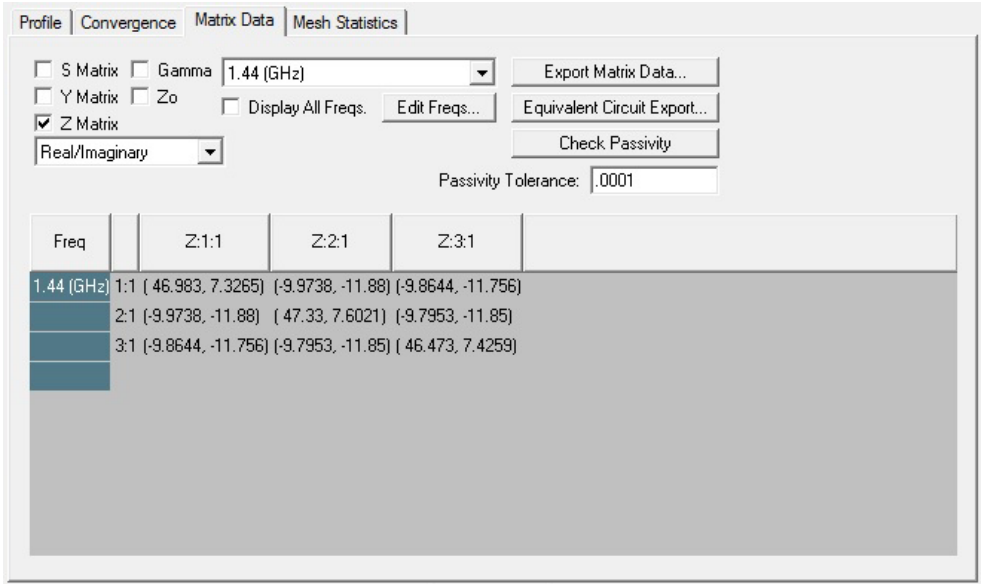

Fig. 2.2: Impedance matrix for the three elements at the center frequency.

This matrix shows that the input impedance of the three elements (z_{11}, z_{22}, z_{33}) is well matched to a port with a characteristic impedance (Zo) of 50 Ω at this frequency. The good match is determined by the fact that these three parameters have a real part that is very close to 50 Ω and an imaginary part that is close to zero. This ultimately means that a matching network is not required for this array.

2.3.4 Reflection Coefficient and Coupling Results

The next results analyzed are the reflection coefficients (s_{11}, s_{22} and s_{33}) and coupling parameters (s_{12}, s_{21}, s_{13}, s_{31}, s_{23} and s_{32}) over frequency. Figure 2.3 shows the three reflection coefficients over a 400 MHz frequency range (from 1.2 to 1.6 GHz).

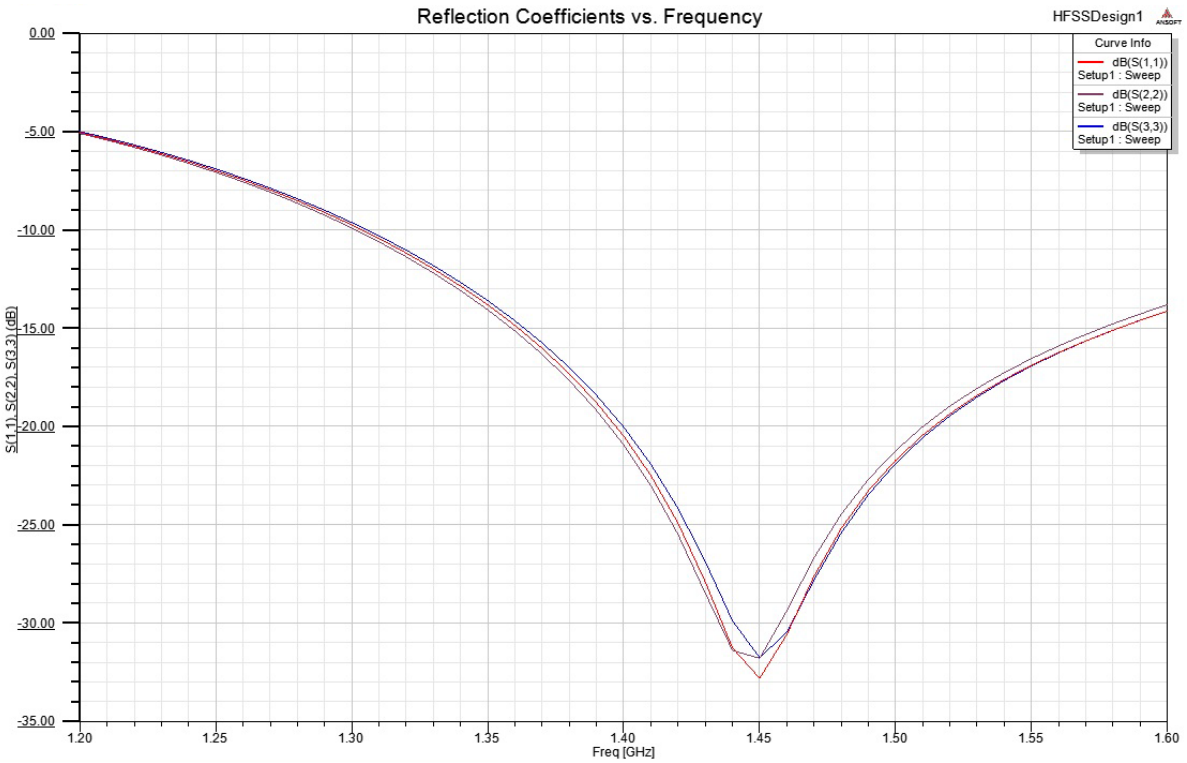

Fig. 2.3: Reflection coefficient vs. frequency for the three elements.

The first thing to notice about these curves is that they are almost overlapping, which is

ideal. The second important thing to notice is that the curves have a minimum value of ~ -32 dB at around 1.45 GHz. This is also good since the reflection coefficients should be as small as possible at the center frequency.

Figure 2.4 shows the six coupling parameters of the array over a 400 MHz frequency range (from 1.2 to 1.6 GHz).

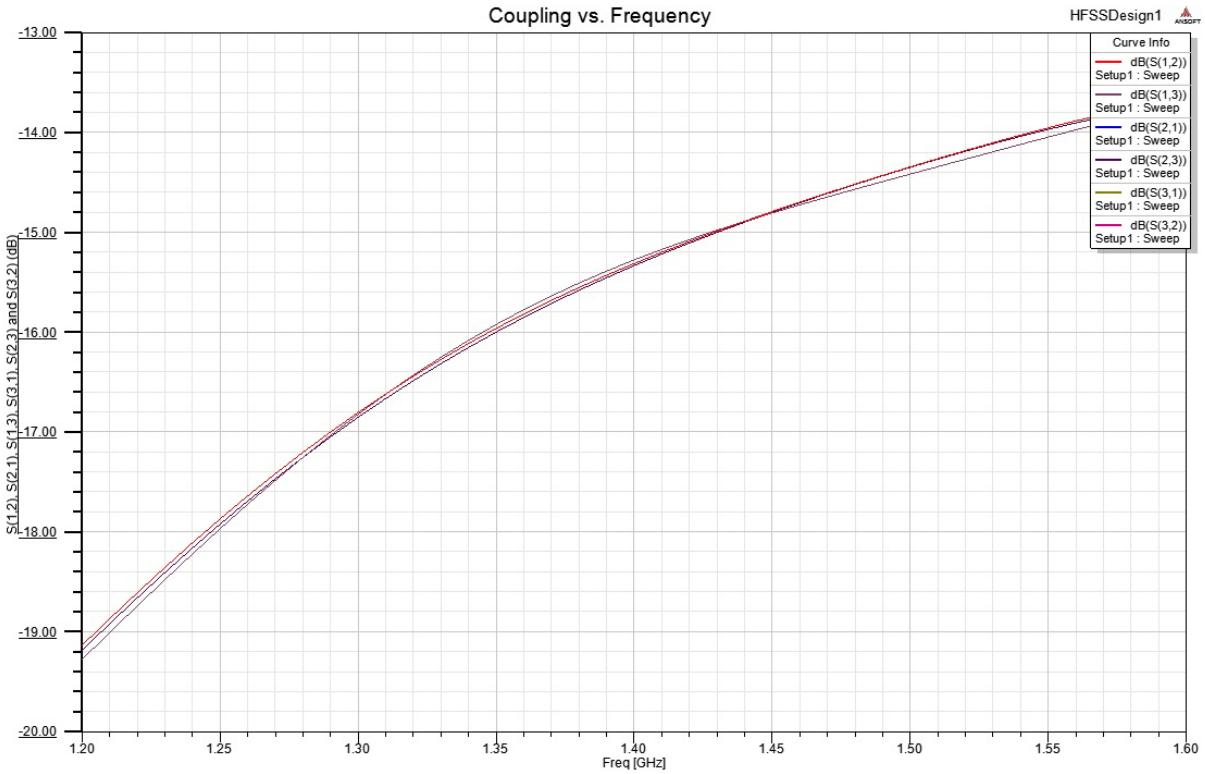

Fig. 2.4: Coupling vs. frequency for the three elements.

The important thing to notice is that all coupling curves have an almost perfect overlap over each other, meaning the network is reciprocal, all the elements dimensions are the same for the three elements and the distances between each other are also the same. It is also important to notice that the coupling level for all the curves is ~ -14.8 dB for the center frequency used in the array and these levels remain below -10 dB for at least the frequency span shown in this window.

2.3.5 Radiation Pattern Results

Determining the radiation pattern of the array required a few more steps than the previous results. First, the array was modified to be only one element located in the origin, instead of the three elements. All other parameters were kept the same. Once this monopole was determined to have a satisfactory radiation pattern, the pattern of the whole array could be determined. Figure 2.5 shows a $\Phi = 0°$ cut of the radiation pattern at 1.4454 GHz of the single monopole with the ground plane.

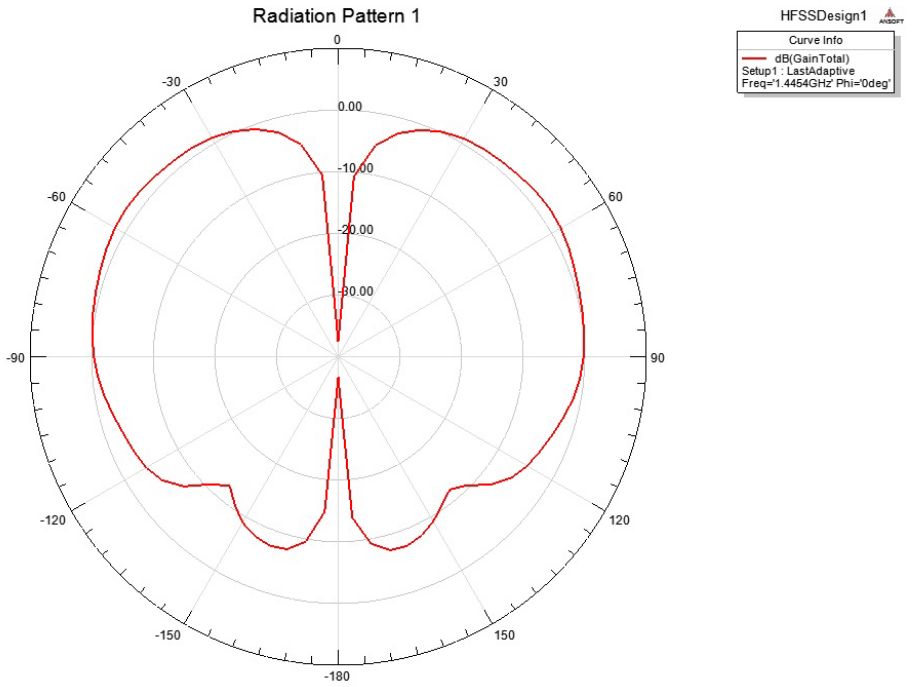

Fig. 2.5: Elevation radiation pattern for 1 monopole.

This pattern shows a maximum gain of ~2 dBi at $\theta = 60°$. It also shows an attenuation for $90° < \theta < 180°$ because of the ground plane. Finally, it also shows a null at $\theta = 0°$ and $\theta = 180°$. All these characteristics agree with theory, so the next step is to use the original array and measure the radiation pattern of each element separately. While the element being analyzed is excited, the other two elements in the array are terminated with 50 Ω loads. By repeating the

process for the three elements, the three radiation patterns can be determined. The following two figures show two of these 3-D radiation patterns. In Figure 2.6, element 2 is being excited and in Figure 2.7, element 1 is being excited.

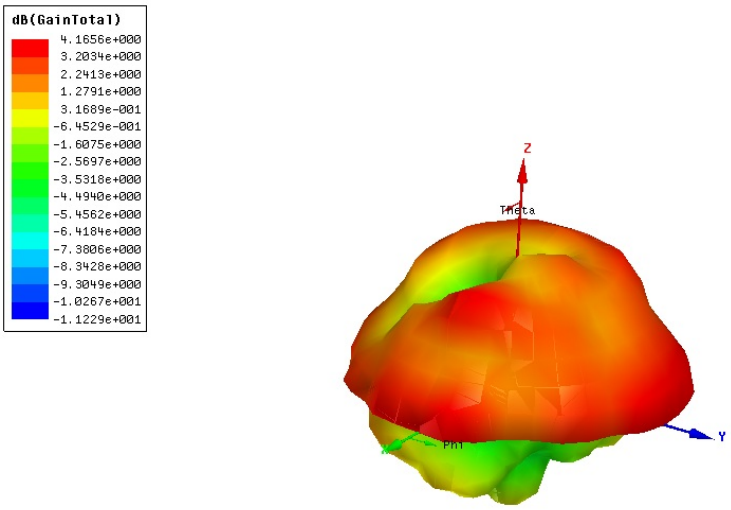

Fig. 2.6: 3-D radiation pattern for element 2.

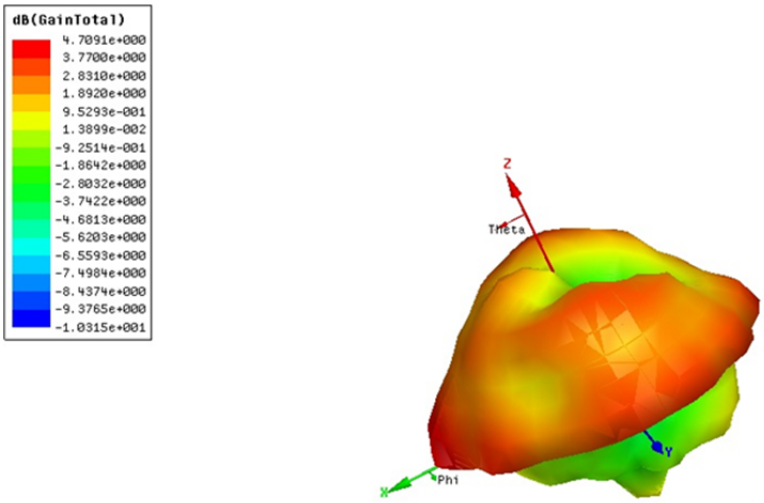

Fig. 2.7: 3-D radiation pattern for element 1.

In these figures, it can be noted that at θ = 90° (the ground plane level), the pattern has a higher gain at the azimuth angle where the excited element is at. The gain is between 4 and 5 dBi at this point (in accordance to theory). At the azimuth angles where the 50 Ω terminated elements

are located at, a slight gain attenuation can be noted. The gain at these points is between 1 and 2 dBi. This is expected since, even though the other two elements are not being excited, they still interfere with the pattern of the element being excited. Finally, it is important to note that the pattern is also attenuated for $90° < \theta < 180°$ because of the ground plane and that the $\theta = 0°$ null is slightly offset since the element being excited is no longer in the origin. Azimuthal and elevation 2-D radiation patterns of element 1 are now included in order to have a better visualization of the exact gain levels on these two planes. Figure 2.8 is its azimuthal radiation pattern with $\theta = 90°$. Figure 2.9 is its elevation radiation pattern with $\Phi = 0°$.

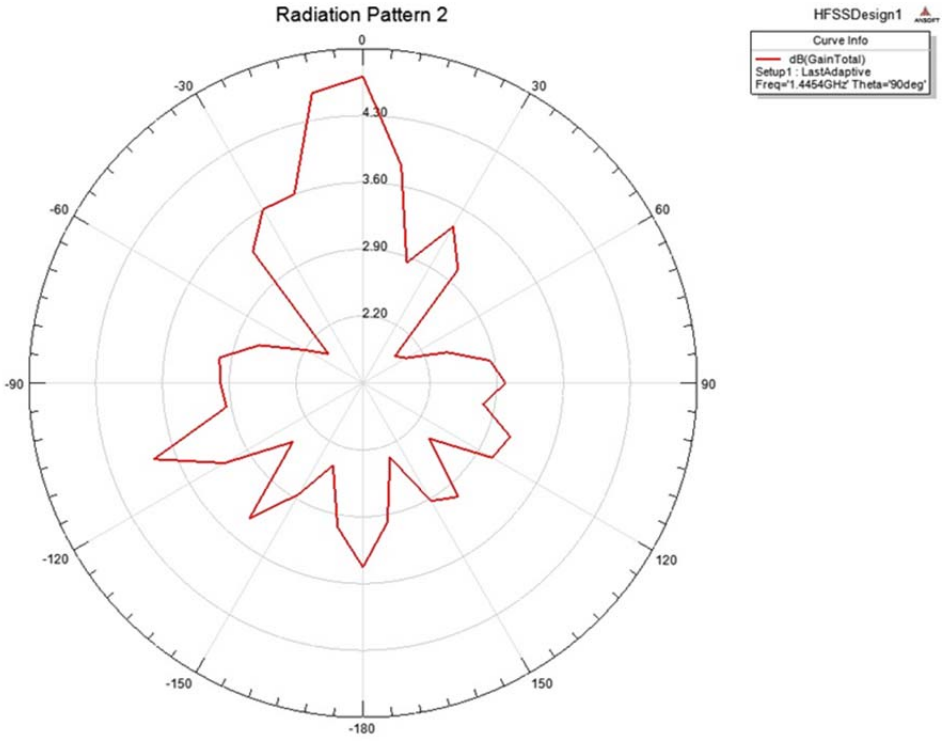

Fig. 2.8: Azimuthal radiation pattern for element 1.

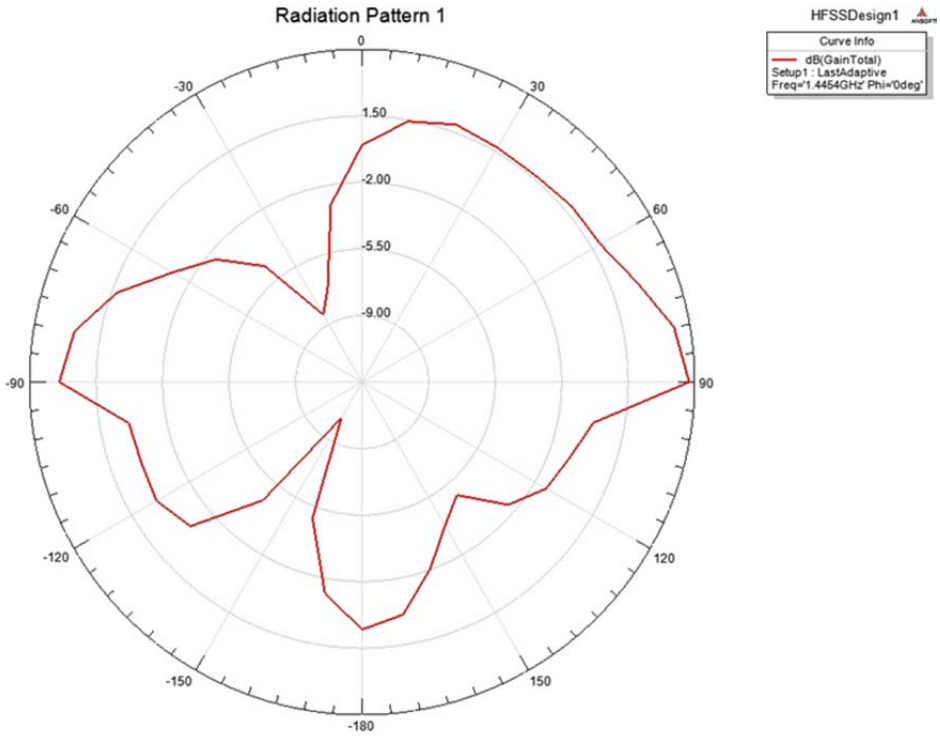

Fig. 2.9: Elevation radiation pattern for element 1.

Notice on the azimuthal radiation pattern that the gain is higher at the azimuthal angle where the element is closest to ($\Phi = 0°$ for element 1) and that at this angle, the gain is ~4.6 dBi. Notice on the elevation radiation pattern that the gain is severely attenuated for $90° < \theta < 180°$ and that the maximum gain occurs at $\theta = \sim 90°$ with a gain of ~4.8 dBi.

2.3.6 s_{21} Results For Relative Gain Calculations

The third HFSS™ setup used was to have the monopole array with a transmitter antenna placed in the far field at different azimuth angles. The far field (r_{ff}) can be calculated using the largest r_{ff} of the following three equations:

$$r_{ff} > \frac{2D^2}{\lambda} \; [m] \qquad (2.1)$$

$$r_{ff} \gg D \; [m]$$

$$r_{ff} \gg \lambda\ [m] \qquad (2.2)$$

(2.3)

where D is the maximum linear dimension of the antenna [18].

Using Equation 2.1, r_{ff} is calculated to start at 2.3 cm away from the antennas. Using Equation 2.2, r_{ff} is calculated to start at 4.9 cm away from the antennas. Using Equation 2.3, r_{ff} is calculated to start at 20.8 cm away from the antennas. Thus, the transmitter antenna is chosen to be placed at 2 m from the origin at four different azimuth angles (θ = 0°, 90°, 180° and 270°) on the same level as the ground plane. The transmitter antenna is a simple monopole centered on a ground plane with the same dimensions as the antennas used in the array. Figure 2.10 shows this setup for when the transmitter is placed at θ = 270°.

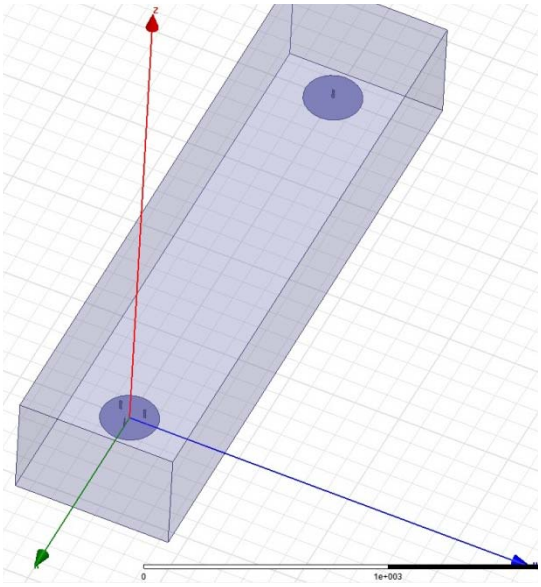

Fig. 2.10: Transmitter-Receiver setup for s_{21} measurement.

This setup is used to measure s_{mn} for the three different receiver antennas, where m equals element 1, element 2 or element 3 (depending on which one is being excited) and n stands for the transmitter antenna. The magnitude of s_{mn} is then equal to the relative gain between the transmitter and the element being excited for the different azimuth angles chosen. The results of

these measurements are shown in Appendix A, with a comparison to theoretical values. As can be seen, the model s_{mn} magnitude results are close to the theoretical results (at ~ -31 dB) except for a fairly large 15 dB discrepancy when element 3 is excited and the transmitter is placed at 2 m in the negative x axis.

3.1 Overview

To be able to mount the receiver antenna array on the outside of the plane, it is necessary to first design an enclosure to cover the whole array and protect it from the weather. This enclosure will cover the three receiver elements that are on the same plane, not the element that is offset, since that element was designed by another member of the project. This protective enclosure needs to be weather resistant, have little electromagnetic interference on the array elements, be aerodynamic, and lightweight. The material chosen was acrylonitrile butadiene styrene (ABS) plastic, due to its relatively low density (1.05 gr/cc at 70º F) [19], hardness, rigidity, no brittleness and a good balance between tensile strength, impact resistance and electrical properties. To make it aerodynamic, the shape chosen for the structure needed to have no sharp edges but still cover the whole array. For this reason, a dome was chosen with a rim around it so that it can be attached to the array. [20]

3.2 Material Properties

Although ABS is usually used for mechanical purposes, it also has good electrical properties that are fairly constant at a wide range of frequencies. These properties are little affected by temperature and atmospheric humidity in the acceptable range of operating temperatures. The table included in Appendix B shows the most important electrical properties of ABS and some other thermoplastics. As can be seen, the dielectric constant (ε_r) of ABS is constant over a very wide range of frequencies. This makes it safe to assume that the ε_r for ABS is 3.0 at 1.4454 GHz. From the table, it can also be seen that ABS's Dissipation Factor (DF) at 1

GHz is 0.005. Thus, it can be estimated to still be 0.005 at 1.4454 GHz. [21] The quality factor (Q) of ABS is the reciprocal of 0.005, or 200. The resonant frequency (ω_o) of ABS is related to Q according to Equation 3.1:

$$Q = \frac{1}{DF} = \omega_0 W / P_r \qquad (3.1)$$

where $\omega_0$is the resonant radian frequency, W is the maximum stored energy and P_r is the radiated power [22].

3.3 Calculation of Interference and Dome Size

3.3.1 Calculation of Radius, Rim Size, and Thickness

Since the array needs to consist of three antennas equally spaced, on the same plane and with a separation of no more than λ/2 (for an accurate azimuth AoA measurement), the minimum dome radius needs to be the diagonal between the origin and the topmost farthest point of the antenna element. A half wavelength separation would be equal to 10.378 cm. In order to minimize coupling, a value that is close to that is chosen: 10 cm. This yields an xy plane separation between the origin and the center of the feed of the antenna element of 5.77 cm. Since the width of the antenna element is 1 cm, 0.5 cm needs to be added to this measurement. The antenna element height, as discussed in Chapter II, is 4.9 cm. The hypotenuse of 4.9 cm and 6.27 cm yields a minimum radius of 7.958 cm. A radius of 10.8 cm is chosen to reduce the amount of power reflected from the dome. This choice is better visualized in Figure 3.1.

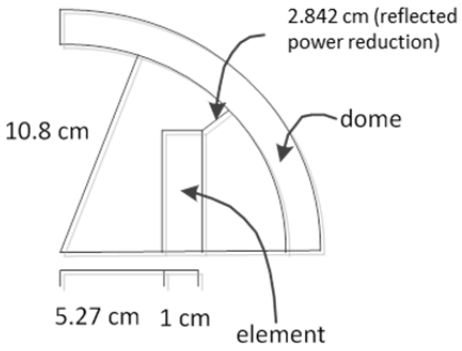

Fig. 3.1: Side view showing the antenna element, ground plane and dome.

A thickness of 0.5 cm ensures that the structure is stable and can protect the array from weather, while keeping the dome structure from being too heavy. Using Google Sketchup®, the final volume of the entire dome with the rim included (a 2.76 cm wide rim with 0.5 cm thickness) is V = 582 cm^3. By multiplying the density of ABS and the volume found, the dome mass is found to be 611 g (1.35 lbs).

3.3.2 HFSS Simulation of Dome's Effects on Radiation Pattern

After importing the dome into HFSS™ as a .stl file, the material properties were assigned to it. Since HFSS does not have ABS as a material, GIL GML 1000TM was chosen as its material due to its close characteristics to ABS. The only property that needed to be changed was its permittivity; changed from 3.12 to 3.0. The final model is shown in Figure 3.2.

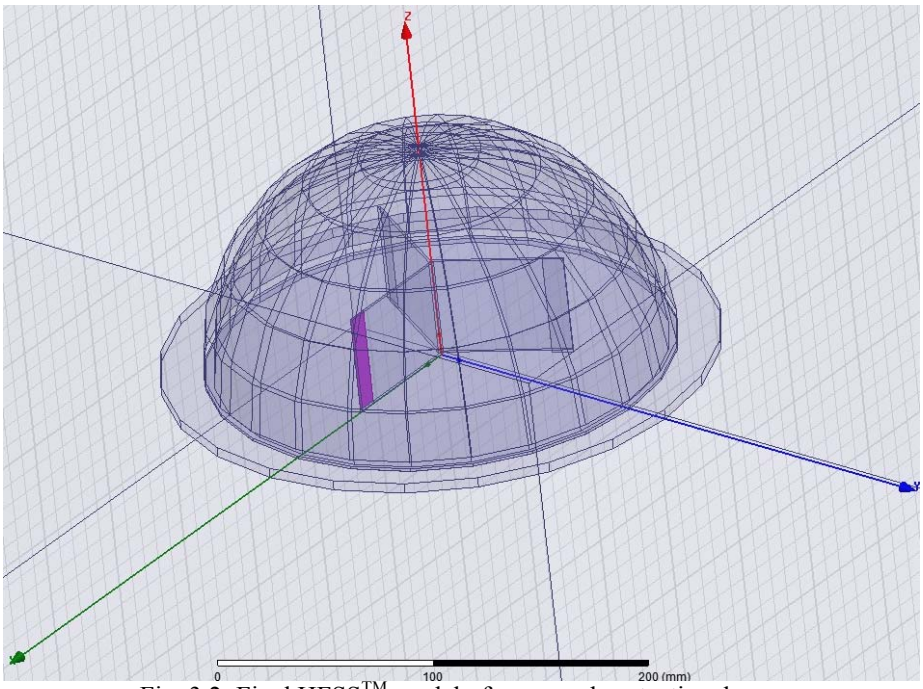

Fig. 3.2: Final HFSS^{TM} model of array and protective dome.

Even though the dome material is non-metal, there is still some interference between the elements and the dome, especially due to their proximity. This can be seen in the 3-D radiation pattern shown in Figure 3.3 for the same element used in Figure 2.7.

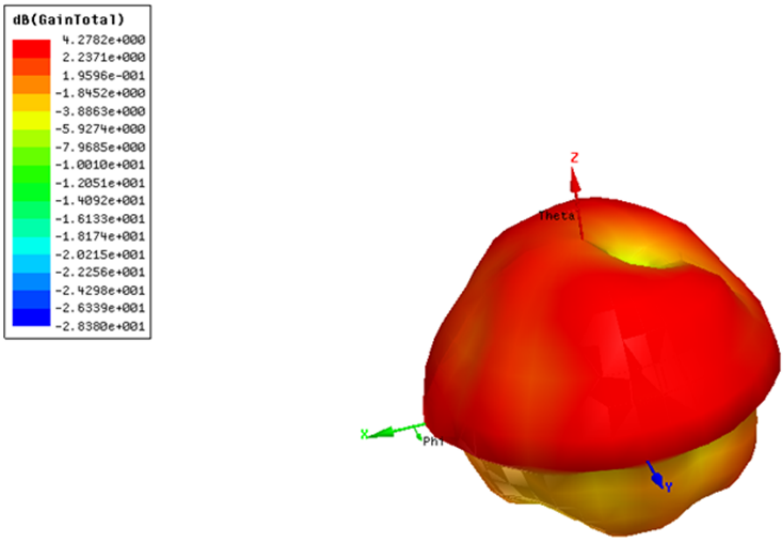

Fig. 3.3: 3-D radiation pattern for element 1.

This 3-D pattern shows an attenuation of ~0.4 dB from its maximum gain level in figure 2.6. This is sufficiently low to be ignored. This small attenuation can be confirmed in the 2-D azimuthal and elevation radiation patterns shown in Figure 3.4 and Figure 3.5, respectively.

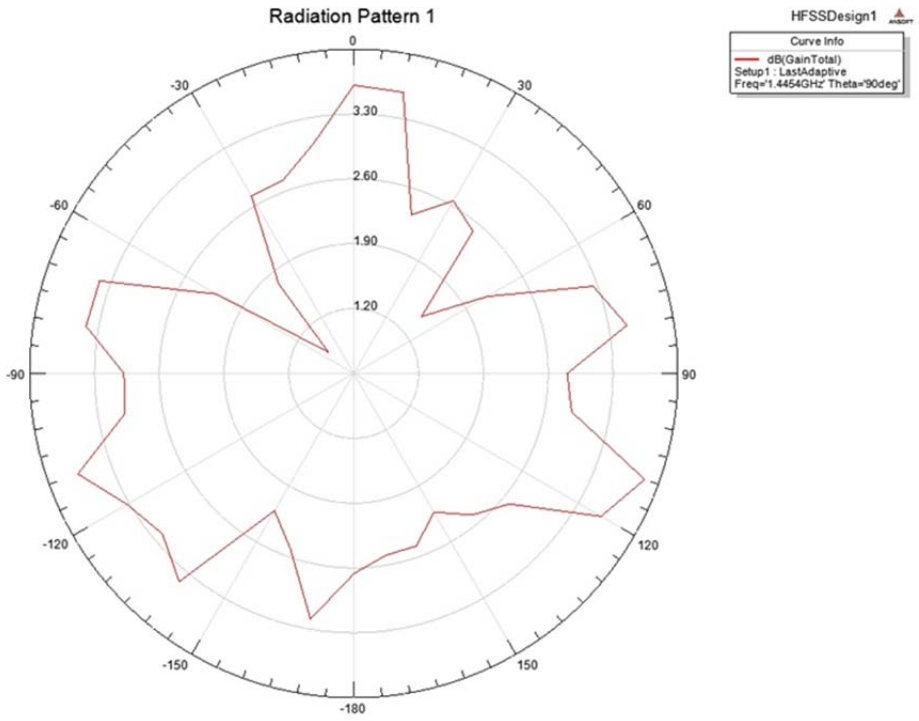

Fig. 3.4: Azimuthal radiation pattern for element 1.

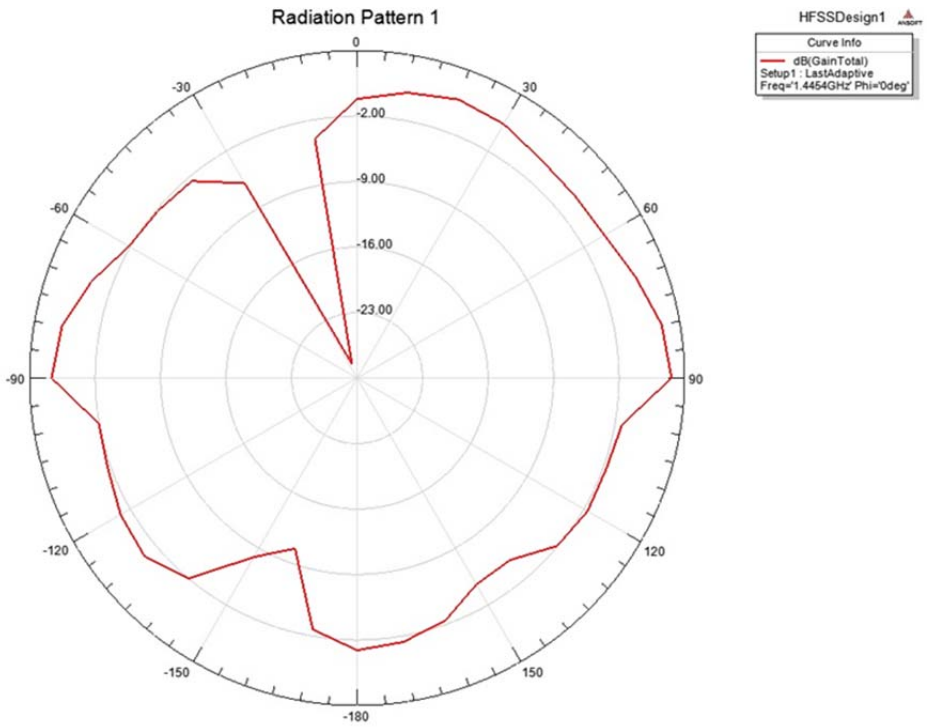

Fig. 3.5: Elevation radiation pattern for element 1.

Comparing the azimuthal pattern with the dome to the azimuthal pattern without the dome in Figure 2.8, it can be seen that the maximum gain has no drastic change: it is still at the about same level (0.6 dB lower than in Figure 2.8) and points in the same azimuthal direction. The shape of the pattern has some minor changes, especially at around $\Phi = 120°$ and -120° but they are also negligible. Comparing the elevation pattern with the dome to the elevation pattern without the dome in Figure 2.9, it can be seen that the maximum gain has only a minor change in level (0.8 dB lower than in Figure 2.9) and no change in direction. Under the ground plane there is an attenuation of about 1 dB. In conclusion, the dome can be placed over the array with no important changes in the radiation pattern.

3.4 Google Sketchup® Modeling

3.4.1 Procedure

Modeling the dome in Sketchup® was an easy process once all the dimensions were determined. First, two quarter circles were made on the same plane, offset by the chosen thickness. They were connected at both ends to form a closed surface. To make the rim, connect a surface with a height of the decided thickness and the length of 2.76 cm that was previously decided on one of the ends of the first surface, on the same plane as the initial surface. Basically, have a quarter circle representing the dome, with a rectangle representing the rim connected to one of the ends of the quarter circle, and give both surfaces a thickness. The final step is to rotate this united surface around 360 degrees.

3.4.2 Final Model

Figure 3.6 shows the final Sketchup® model.

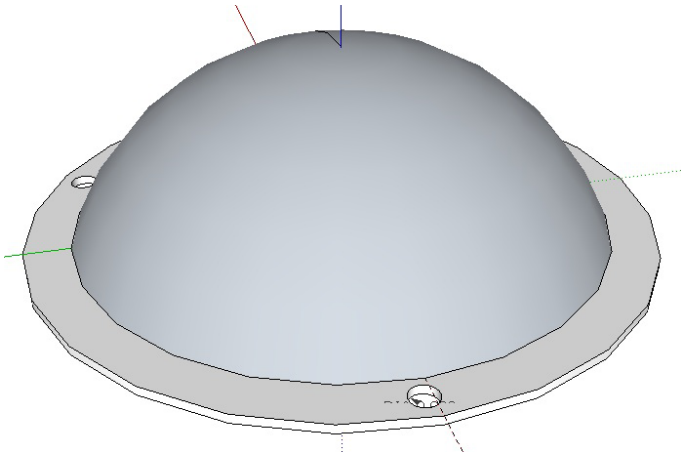

Fig. 3.6: Final Sketchup® model.

3.5 Building Process

3.5.1 3-D Printer and Challenges

The printer used to print the protective dome is the Makerbot Replicator™. This printer has a build envelope of 225 x 145 x 150 mm and can have ABS plastic as its printing material. Due to the printer dimensions, the protective dome needs to be printed in halves so that it fits within the build envelope. The file type from Sketchup® (.skp) needs to first be converted to a .stl file so that it can be used in the 3-D printer. After numerous attempts to print the dome, it still had a severe warping. This warping could not be fixed, but a smaller, scaled version a quarter of the dome could be printed with no major issues.

3.5.2 Protective Dome-Scaled Version

Figure 3.7 shows the final printed ABS plastic quarter dome.

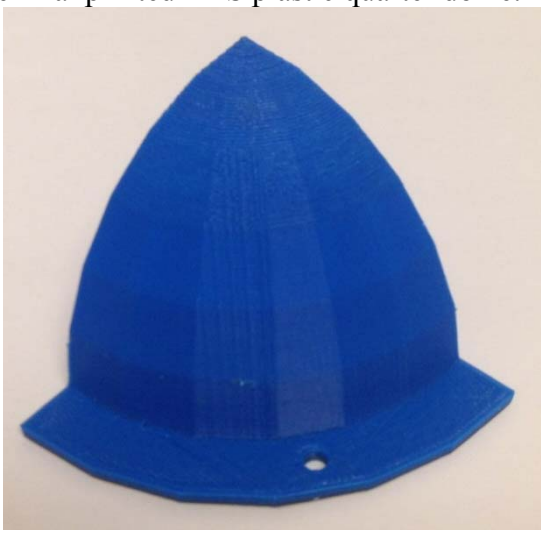

Fig. 3.7: 3-D printed ABS plastic quarter dome.

4.1 Building Process

4.1.1 Eagle® software

Building a printed circuit board (PCB) in Eagle® usually requires an initial schematic design followed by a board design. In the board design, all the components and connections are arranged on the physical board. Due to the relative simplicity of both the ground plane and the three PCBs used for the monopole supports, the schematic design part can be skipped. After these four PCBs are designed, the seven gerber files (top and bottom copper, top and bottom solder mask, top and bottom silkscreen and the drill file) are created. These seven files are used in the milling machine to create the PCB.

4.1.2 Milling Process and Final Building Steps

The University of Kansas' EECS Shop uses LPKF's ProtoMat S62 as its milling machine. The PCB sheets used for this project are 53 mils thick one sided FR-4 sheets. The copper thickness on these sheets is 1.34 mils (1-ounce copper). Once the milling machine finished its milling process, three holes were drilled in the ground sheet. These holes are right below where the three monopoles are placed (centered about the origin of the ground plane and 10 cm away and 120° apart from each other) and need to be wide enough to pass the SubMiniature version A (SMA) male connector feeds, which are placed on the copper side of the ground plane, since the FR-4 side faces the three monopoles. After the SMA male connectors are soldered to the ground plane and the feeds are passed through the three drilled holes in the ground plane, the FR-4 sheets with the monopoles are soldered to the SMA feeds, vertical to the ground plane. Finally,

the three vertical FR-4 sheets are glued to each other along the axis where the three of them meet using epoxy glue. Finally, the solder between the SMA connectors and the ground plane was smoothed out using a hot air blower. A top and bottom view of the final antenna array are shown in Figure 4.1 and Figure 4.2, respectively.

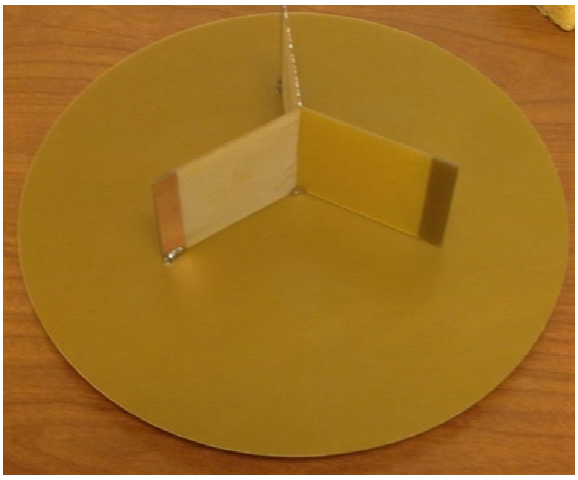

Fig. 4.1: Top view of final monopole array showing the three monopoles.

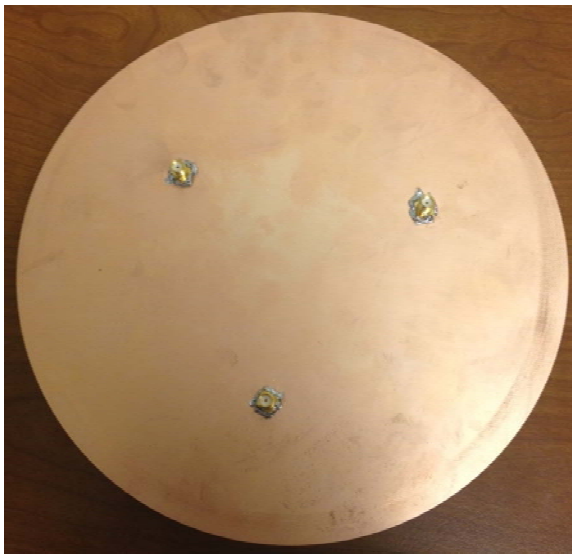

Fig. 4.2: Bottom view of final monopole array showing the three SMA connectors.

4.2 Preliminary Measurements

4.2.1 Reflection Coefficient Measurements

Due to a restricted access to The University of Kansas' anechoic chamber, preliminary measurements of the monopoles' reflection coefficient, coupling and gain were made in a lab using a network analyzer. These measurements are simple rough estimates so that the results achieved using HFSS^{TM} can be compared to actual results. The final measurements were taken in the anechoic chamber.

After properly calibrating the network analyzer, the reflection coefficients for the three elements were measured over frequency by connecting port 1 of the network analyzer to the element being measured and terminating the other two with 50 Ω loads. Figure 4.3 shows the magnitude of s_{11} versus a frequency range of 1 GHz (from 1 to 2 GHz).

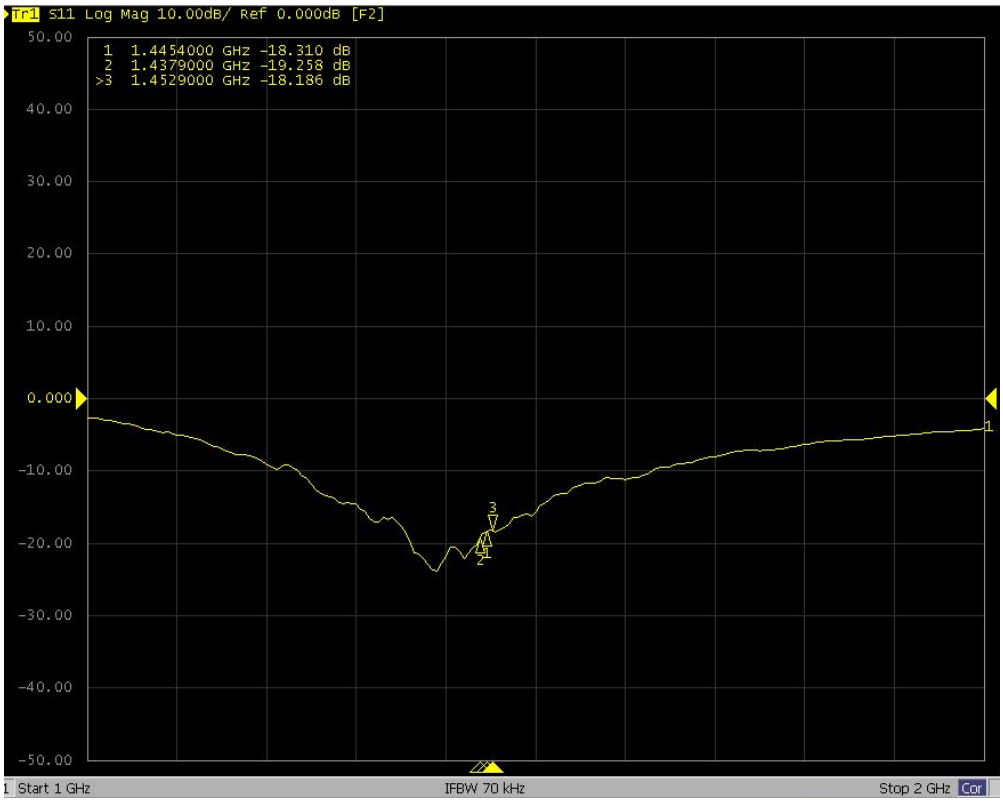

Fig. 4.3: Magnitude of s_{11} from 1 to 2 GHz.

These results show that, at the center frequency, the magnitude of s_{11} is -18.3 dB. The other two markers in the curve are placed at +/- 7.5 MHz from the center frequency. The reflection coefficients at these marker frequencies are -18.2 dB and -19.3 dB, which are still fairly low levels, meaning that the reflection levels are good for this frequency span. In fact, for frequencies ranging from 1.2 GHz to about 1.6 GHz, the reflection levels are below -10 dB. One important thing to note is that the minimum level (~ -24 dB) is at a frequency lower than the center frequency, at around 1.38 GHz. This means that the antenna element is slightly longer than it should. Even though these results are important for reflection coefficient estimates, the measurements were taken in a very noisy environment with a many sources of interference. Depending on the orientation of the antenna and how close other surfaces are to it, the values changed by up to 5 dB. Figure 4.4 shows the s_{11} magnitude versus a frequency range of 30 MHz.

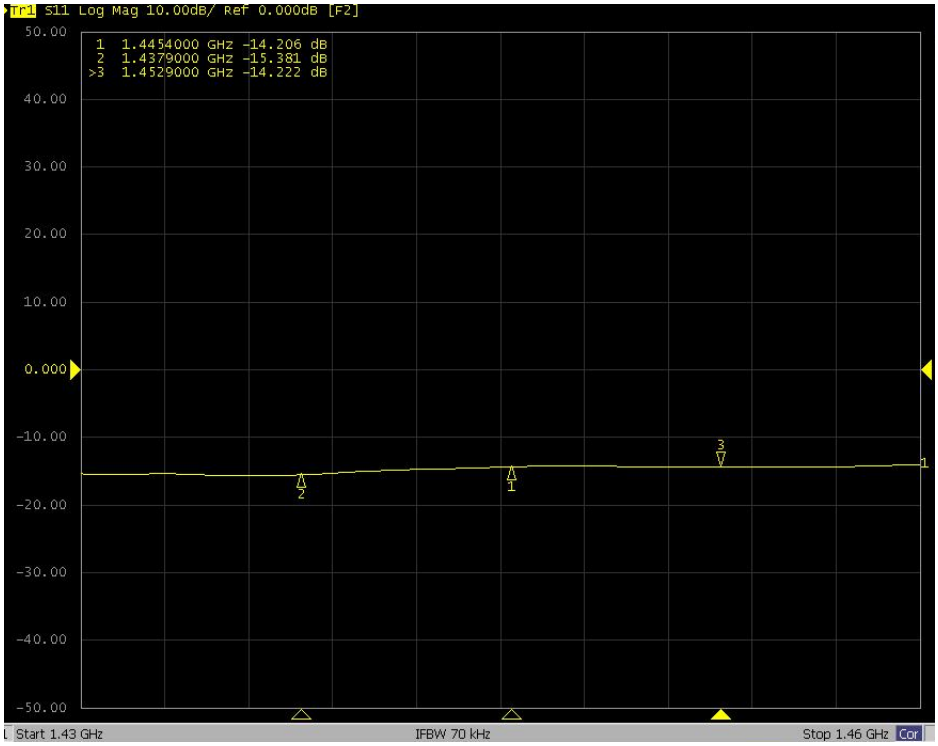

Fig. 4.4: Magnitude of s_{11} from 1.43 to 1.46 GHz.

Note that, even though the reflection coefficients is still at a good level (less than -10 dB), there was a ~4 dB variation from the previous results (even though the antenna was the same) in both the center frequency and at the two other markers at +/- 7.5 MHz. The s_{22} and s_{33} reflection coefficient versus the same frequency range results are included in Figure 4.5 and Figure 4.6, respectively, to show that the curve shapes and levels are the same for the three elements.

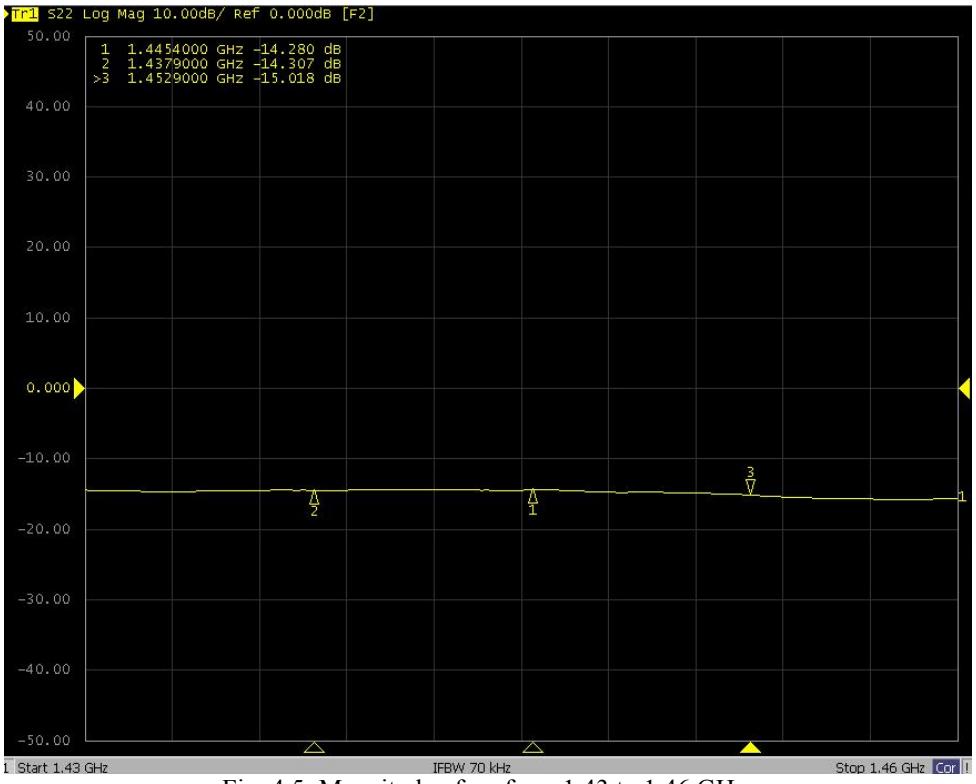

Fig. 4.5: Magnitude of s_{22} from 1.43 to 1.46 GHz.

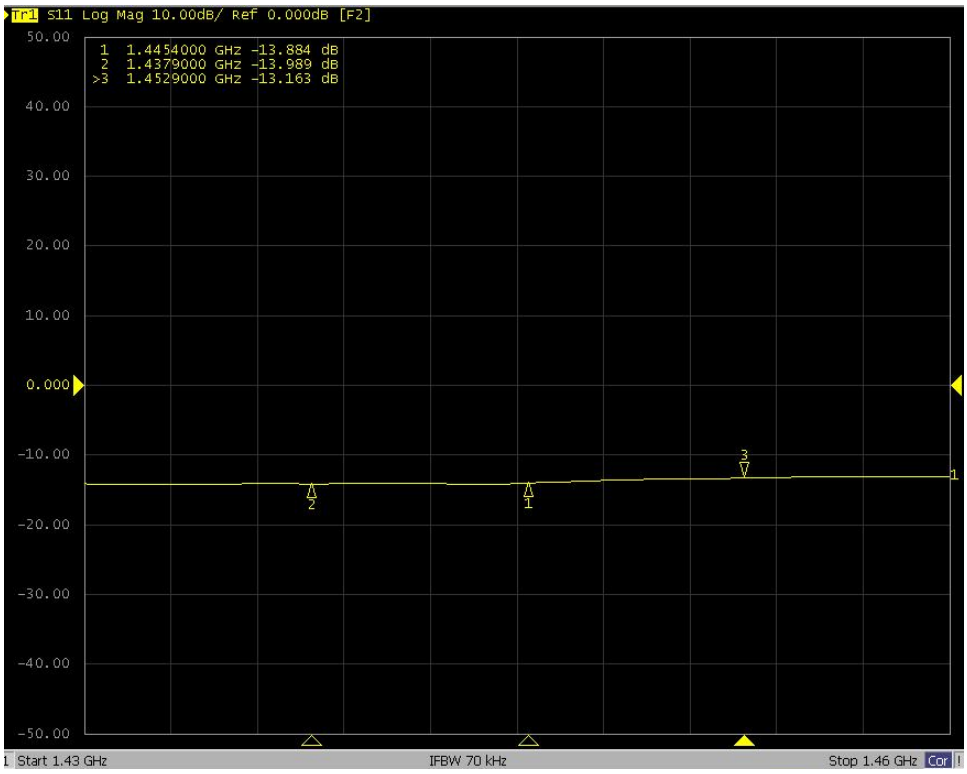

Fig. 4.6: Magnitude of s_{33} from 1.43 to 1.46 GHz.

Comparing these results to the HFSS™ results, the curve shapes are similar, with one main difference: the minimum levels in the HFSS™ results are ~ -32 dB and occur at ~1.4454 GHz, while the minimum levels in the lab results are ~ -24 dB and occur at ~1.38 GHz.

4.2.2 Coupling Measurements

The next measurements taken are for coupling (s_{21}, s_{12}, s_{31}, s_{13}, s_{32} and s_{23}) over frequency. Since the network is reciprocal, only s_{21}, s_{31} and s_{32} were analyzed. The markers were again set at the center frequency and at +/- 7.5 MHz from it. The frequency span analyzed is still 30 MHz (from 1.43 to 1.46 GHz). The results at the center frequency are expected to be between the values of the two curves from figure 2.4 in the HFSS™ results since the cross sectional area value between any two antennas in the built array is between the cross sectional areas of elements 2-3 (minimum cross sectional area) and elements 1-2 and 2-3 in the array modeled in

HFSS^{TM}. The s_{21}, s_{31} and s_{32} curves versus frequency are shown in Figure 4.7, Figure 4.8 and Figure 4.9, respectively.

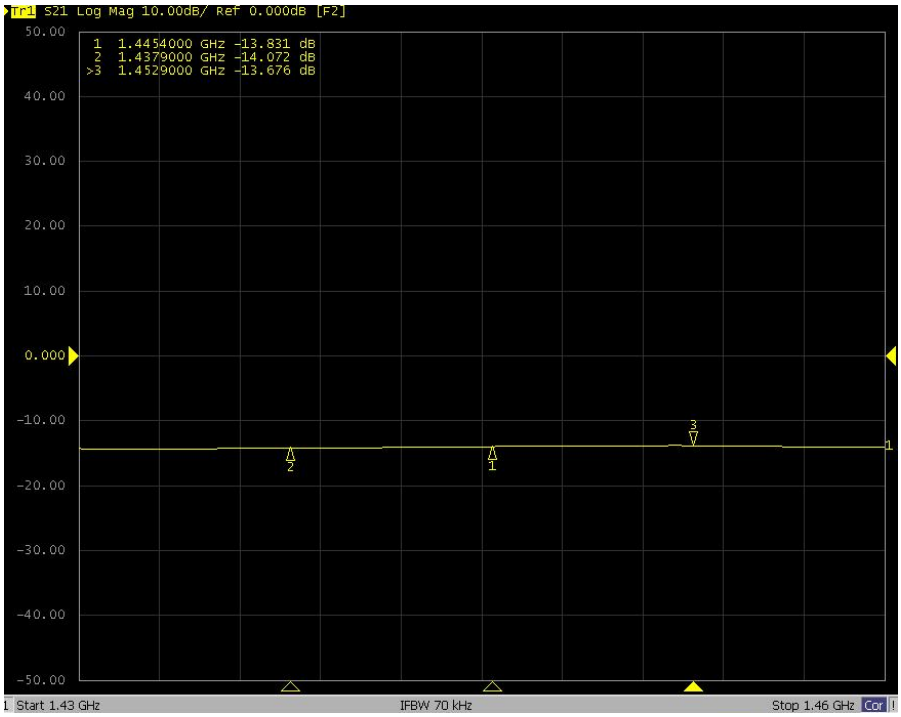

Fig. 4.7: Magnitude of s_{21} from 1.43 to 1.46 GHz.

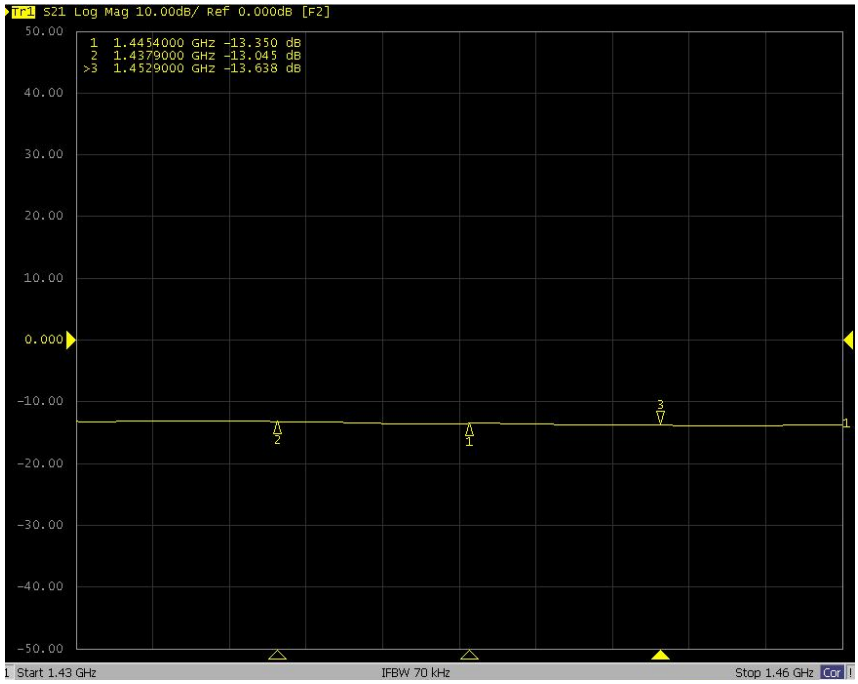

Fig. 4.8: Magnitude of s_{31} from 1.43 to 1.46 GHz.

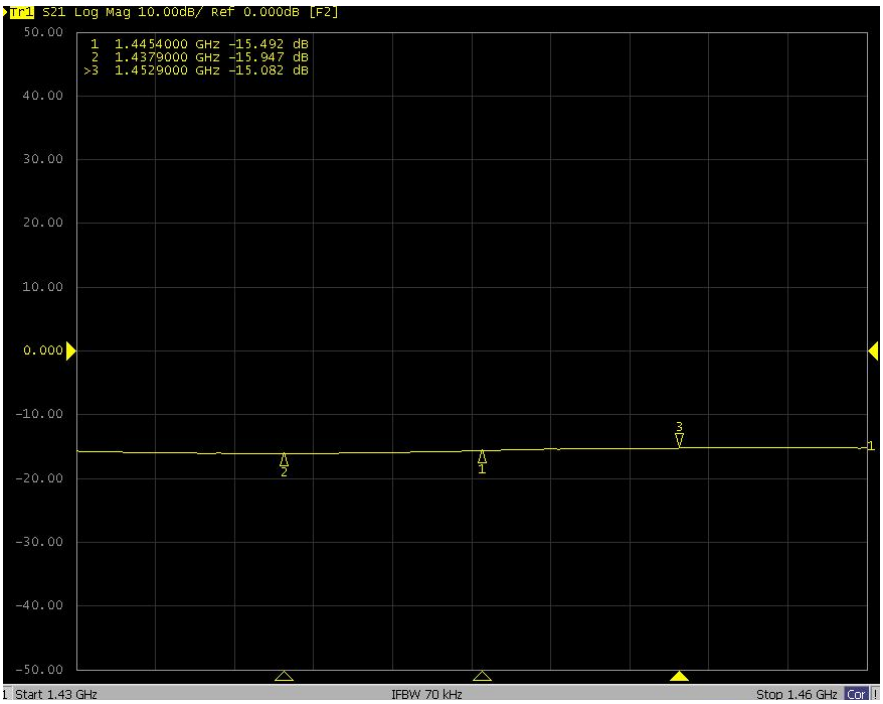

Fig. 4.9: Magnitude of s_{32} from 1.43 to 1.46 GHz.

As it can be seen, the coupling magnitude values at the center frequency are -13.8 dB, -13.4 dB and -15.5 dB, respectively, for the three figures above. These results are very close to the ~ -14.8 dB level for the coupling set by the HFSS™ results. Again, these results are simply estimates since the values are severely affected by noise and other interferences, so the small discrepancies should not be a major concern.

5.1 Measurement of Reflection Coefficients

The reflection coefficient and coupling measurements were not taken inside the chamber, but were made using a more accurate network analyzer (N5230C), with a setup designed to avoid the high level of interference that was observed in the preliminary measurements. For example, the cables used were longer, and this enabled a higher separation between the array and other conducting surfaces in the lab.

Figures 5.1, 5.2 and 5.3 show, respectively, s_{11} and s_{22} and s_{33} versus a frequency range of 150 MHz (from 1.35 GHz to 1.5 GHz).

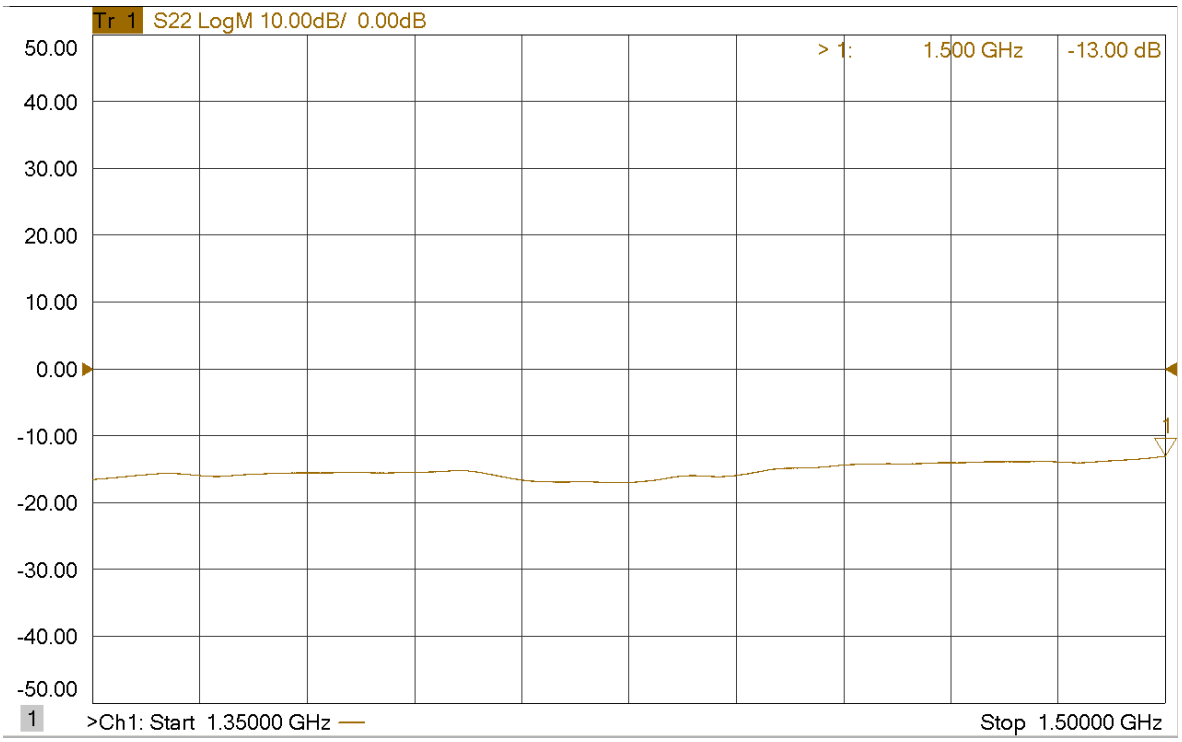

Fig. 5.1: Final measurement of the magnitude of s_{11} from 1.35 to 1.5 GHz.

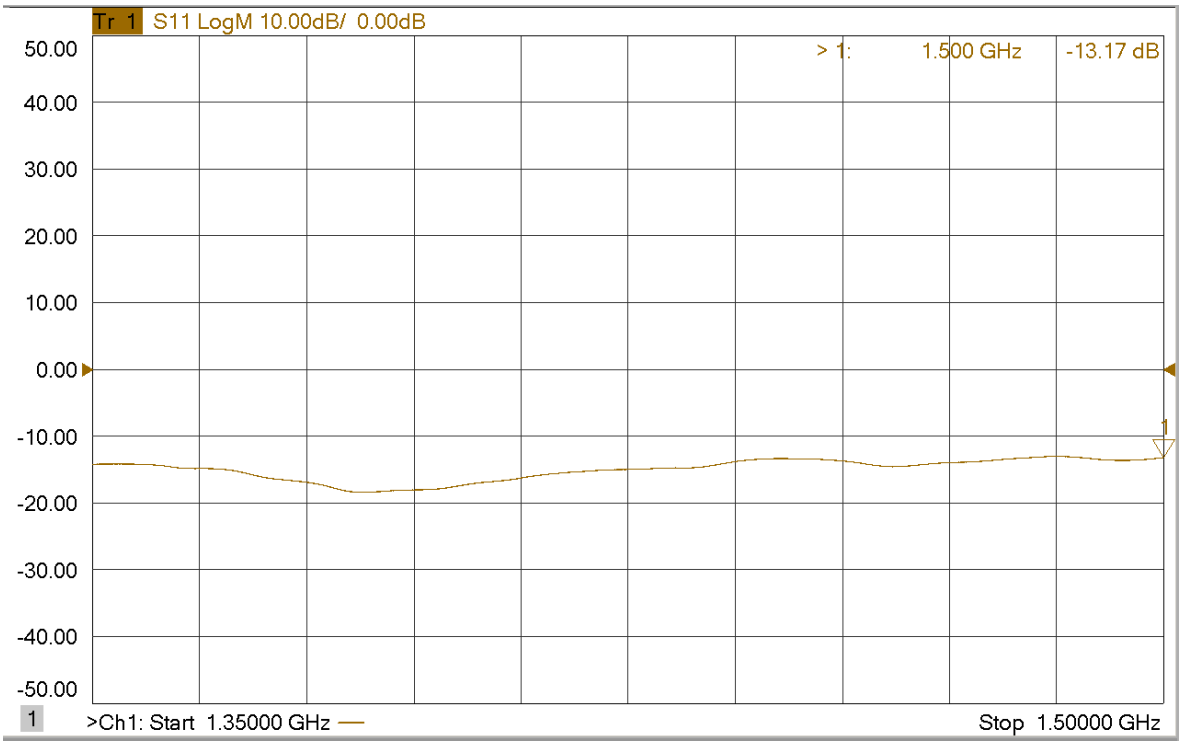

Fig. 5.2: Final measurement of the magnitude of s_{22} from 1.35 to 1.5 GHz.

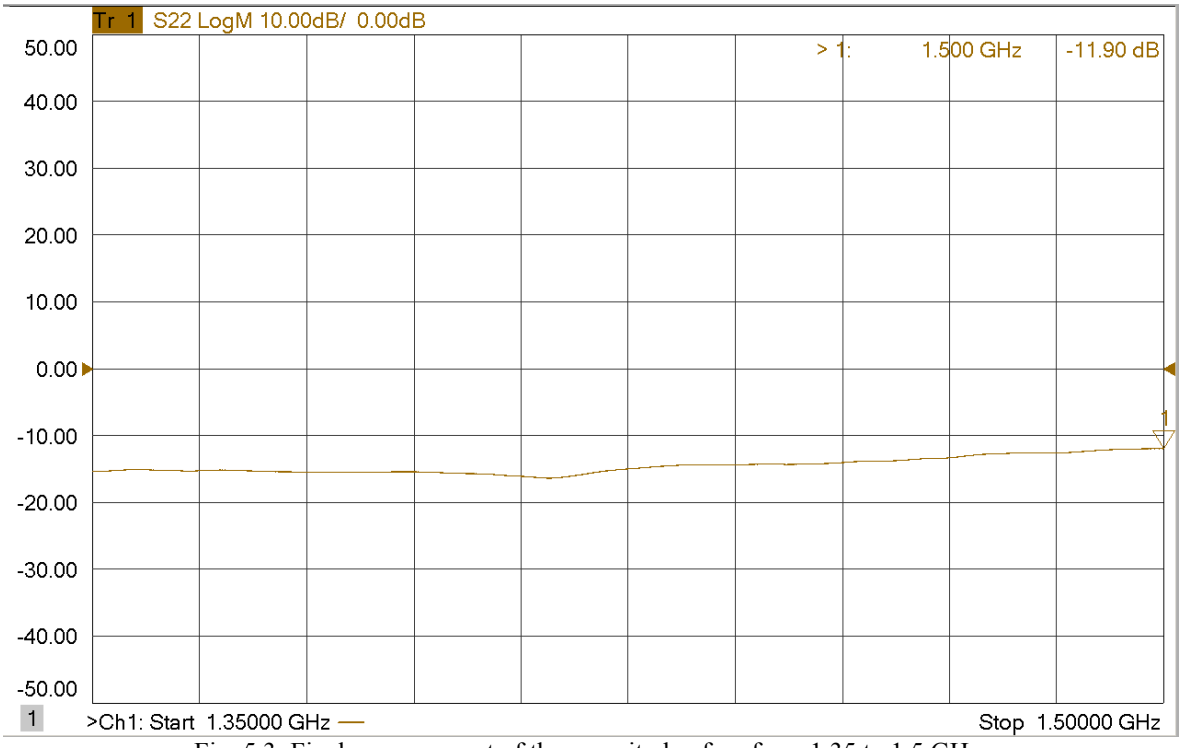

Fig. 5.3: Final measurement of the magnitude of s_{33} from 1.35 to 1.5 GHz.

Even though these graphs do not show the characteristic “v” shaped curve seen in the

HFSS^{TM} results and the results from the other lab, the reflection coefficient levels at the entire frequency range are below -10 dB. For the s_{11} curve, it can be seen that the reflection coefficient is ~ -15 dB at 1.4454 GHz. For the s_{22} curve, it can be seen that the reflection coefficient is ~ -13 dB at 1.4454 GHz. For the s_{33} curve, it can be seen that the reflection coefficient is ~ -14 dB at 1.4454 GHz. These levels are ~18 dB higher than the simulations levels in HFSS^{TM}, but match the levels found using the other network analyzer.

5.2 Measurement of Coupling Coefficients

Figure 5.4, Figure 5.5 and Figure 5.6 show, respectively, s_{21} and s_{31} and s_{32} versus a frequency range of 150 MHz (from 1.35 GHz to 1.5 GHz).

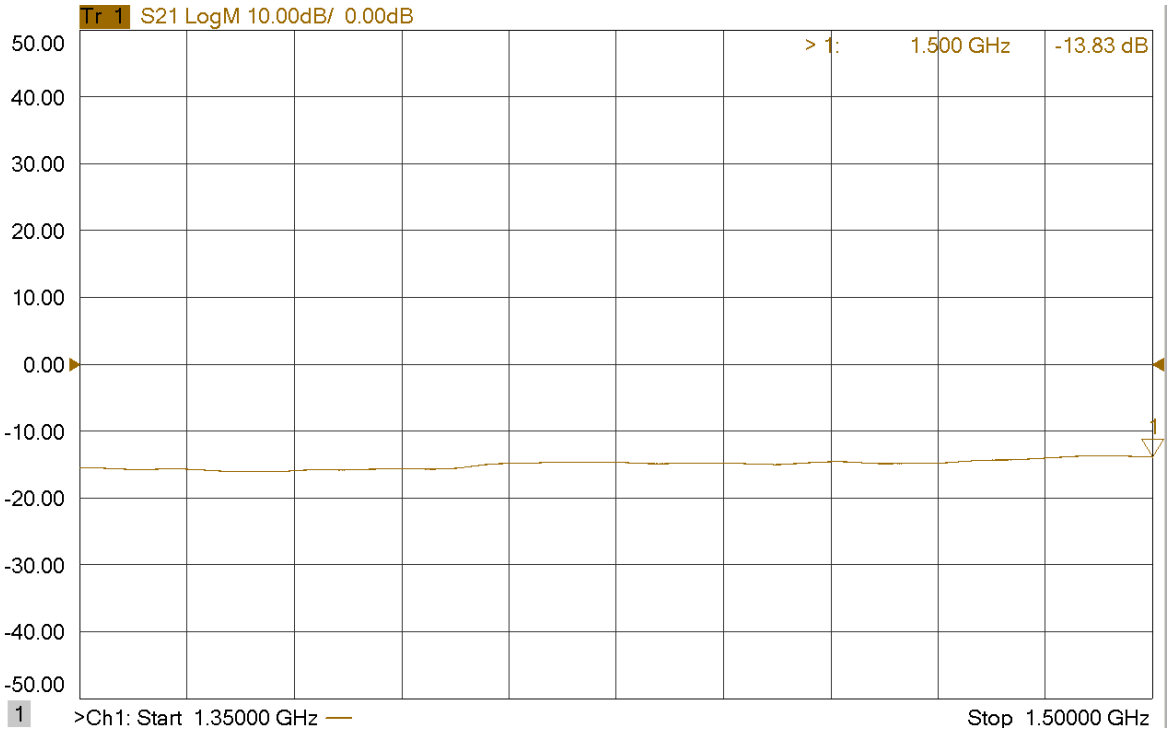

Fig. 5.4: Final measurement of the magnitude of s_{21} from 1.35 to 1.5 GHz.

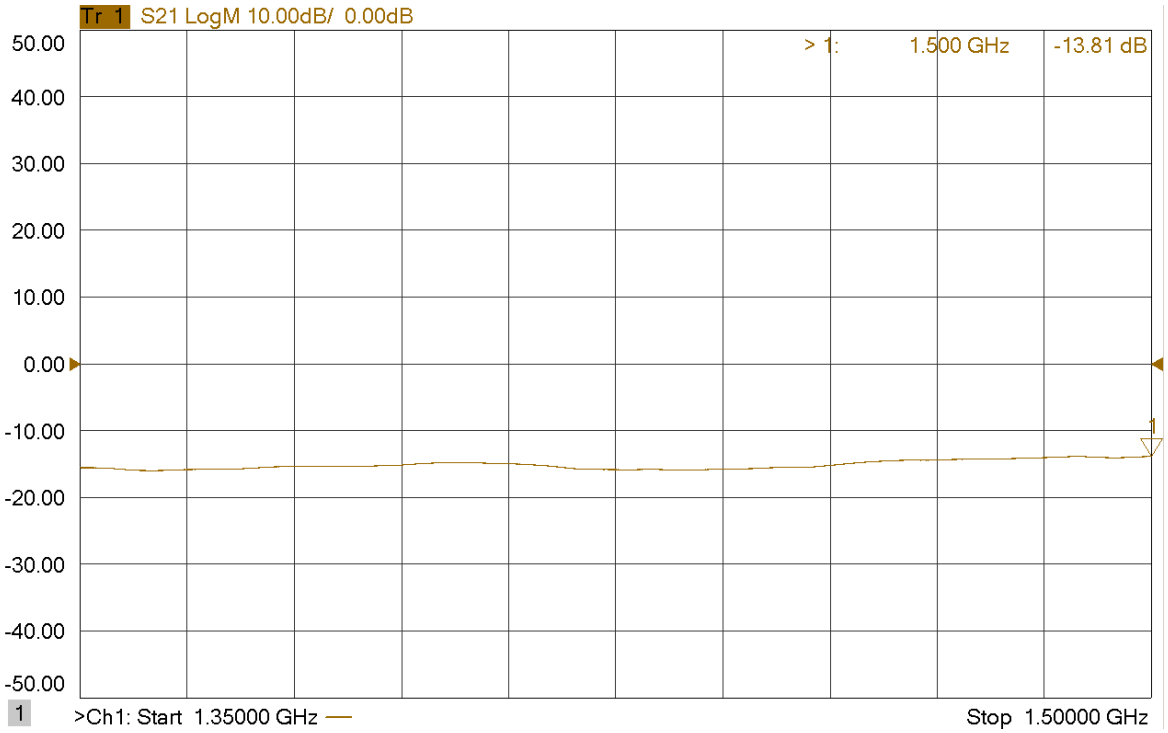

Fig. 5.5: Final measurement of the magnitude of s_{31} from 1.35 to 1.5 GHz.

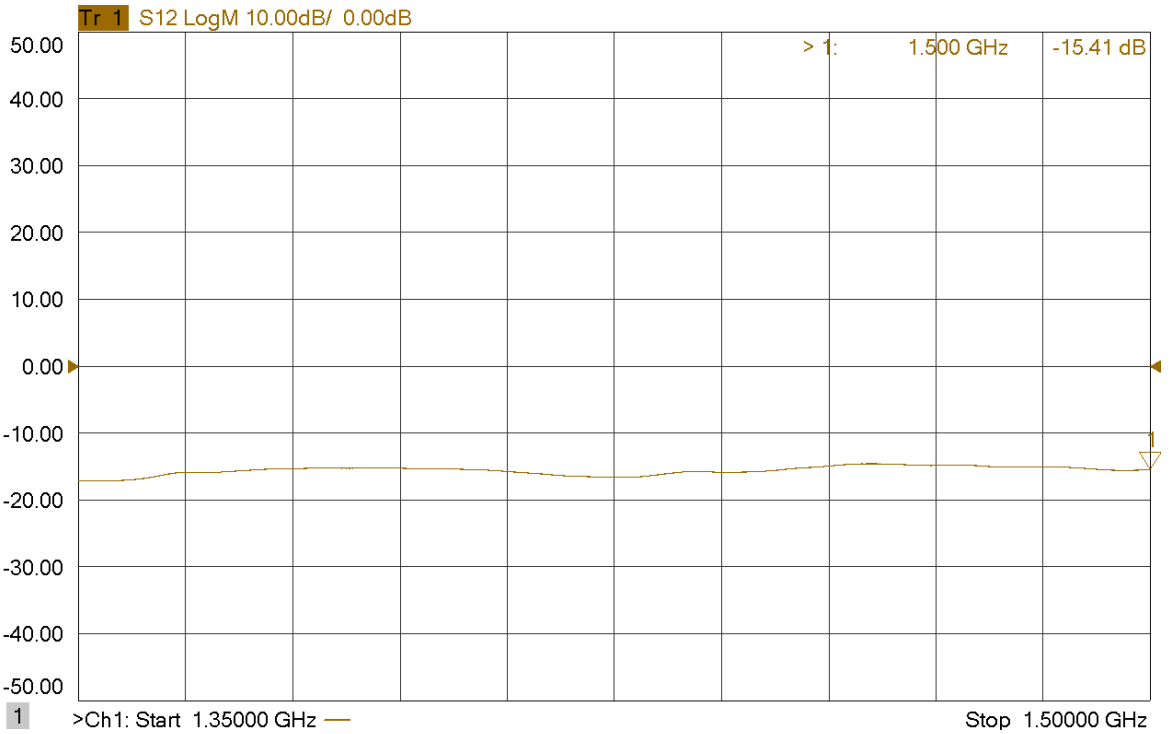

Fig. 5.6: Final measurement of the magnitude of s_{32} from 1.35 to 1.5 GHz.

The coupling level for the three elements is between -15 and -16 dB for the 1.4454 GHz

center frequency and below -10 dB for the entire frequency range tested. These levels are about 1 dB lower than the measurements taken in the other lab and roughly the same as the simulation levels from HFSS™.

5.3 Measurement of Antenna Array Radiation Pattern

5.3.1 Setup

The measurement of the radiation pattern in the anechoic chamber was done using a horn antenna as the transmitter and the monopole array as the receiver. The horn antenna used is Scientific-Atlanta's 12-1.1 Standard Gain Horn. This antenna has a frequency range from 1.1 to 1.7 GHz and a nominal gain of 15.5 dBi [23]. It is mounted 1.29 m from the ground (distance to center of the horn aperture). The monopole array is initially placed 5.7 m away from the transmitter, 1.5 m from the ground on a rotating turntable that rotates 360° in azimuth. One important thing to note about the turntable is that it has a vertical mast that is used to place the antenna array on, but this mast is not located in the center of the turntable. It is at ~0.2 m from the center of the turntable. This means that the range will actually be 5.7 ± 0.2 m and, therefore, the gain measurements will be slightly affected by this offset. Using Equations 5.1, 5.2 and 5.3 and assuming that the transmitter antenna gain is 15.5 dBi and the receiver antenna gain is 5.15 dBi, the inaccuracy in gain is estimated to be ± 0.3 dB [24].

$$\frac{P_r}{P_t} = G_r G_t \left(\frac{\lambda}{4\pi R}\right)^2 \qquad (5.1)$$

$$Insertion\ Loss = 10\log\left(\frac{P_t}{P_r}\right) = -20log(s_{21}) \qquad (5.2)$$

$$s_{21}(dB) = 20log|s_{21}|$$

(5.3)

where P_r is the received power, P_t is the transmitted power, G_r is the nominal gain of the receiver and G_t is the nominal gain of the transmitter.

The initial position of the monopole array in relation to the horn antenna is shown in Figure 5.7.

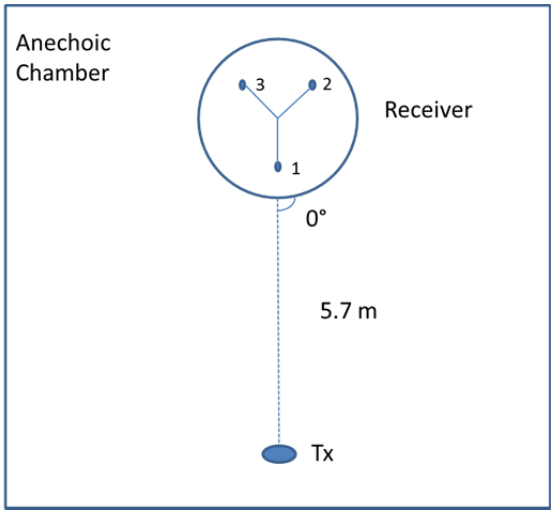

Fig. 5.7: Initial position of monopole array in relation to transmitter antenna in the anechoic chamber.

Using this setup and assuming element Tx to be the transmitter antenna, 1 to be monopole receiver array element 1, 2 to be receiver element 2 and 3 to be receiver element 3, the magnitude and phase of s_{tx1}, s_{tx2} and s_{tx3} is measured for 360° with a 1° resolution. A frequency span of 150 MHz, from 1.35 to 1.5 GHz, with a resolution of 5 MHz is used for these measurements.

This setup yields a relative gain ($G_{relative}$) between the antenna transmitter and each monopole receiver element. To find the gain of the antenna under test (G_{AUT}), the gain of a reference antenna (G_{REF}) needs to be found. G_{AUT} is then given by Equation 5.4 [25]:

$$G_{AUT} = G_{REF} + G_{Relative} \qquad (5.4)$$

This equation is applied to each measurement point in the 360° azimuth coverage.

5.3.2 Results

The gain and phase patterns for element 1 are given in polar plots for θ = 90° and 0° < Φ < 360° and a frequency of 1.44525 GHz (trace frequency closest to the center frequency used) in Figure 5.8 and Figure 5.9, respectively.

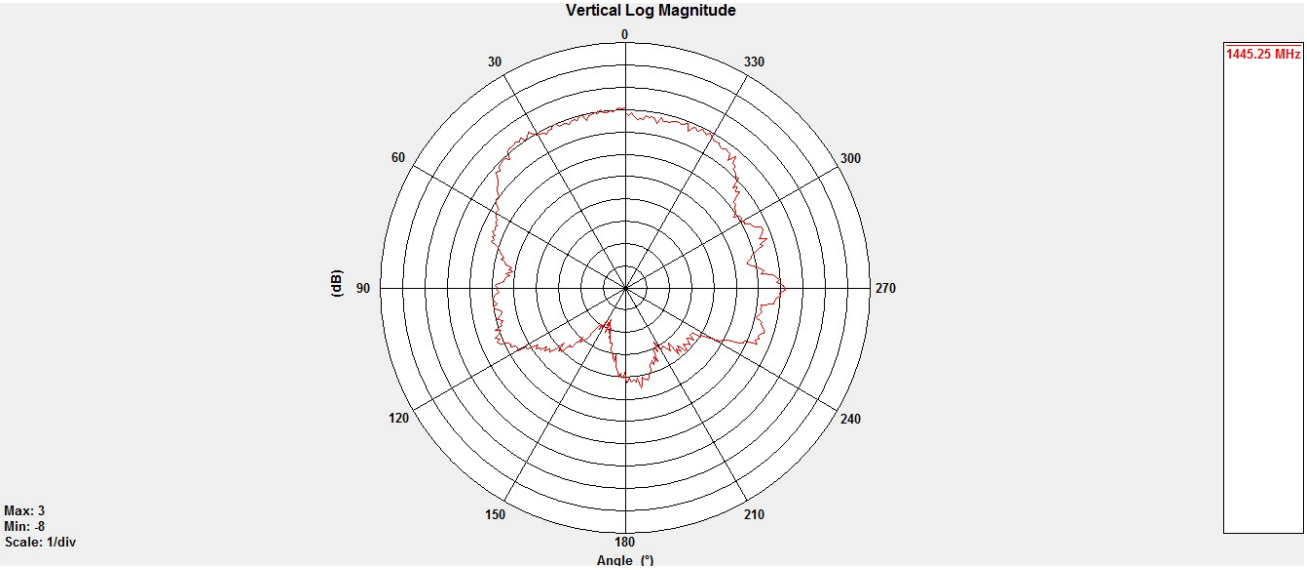

Fig. 5.8: Azimuthal gain radiation pattern for element 1.

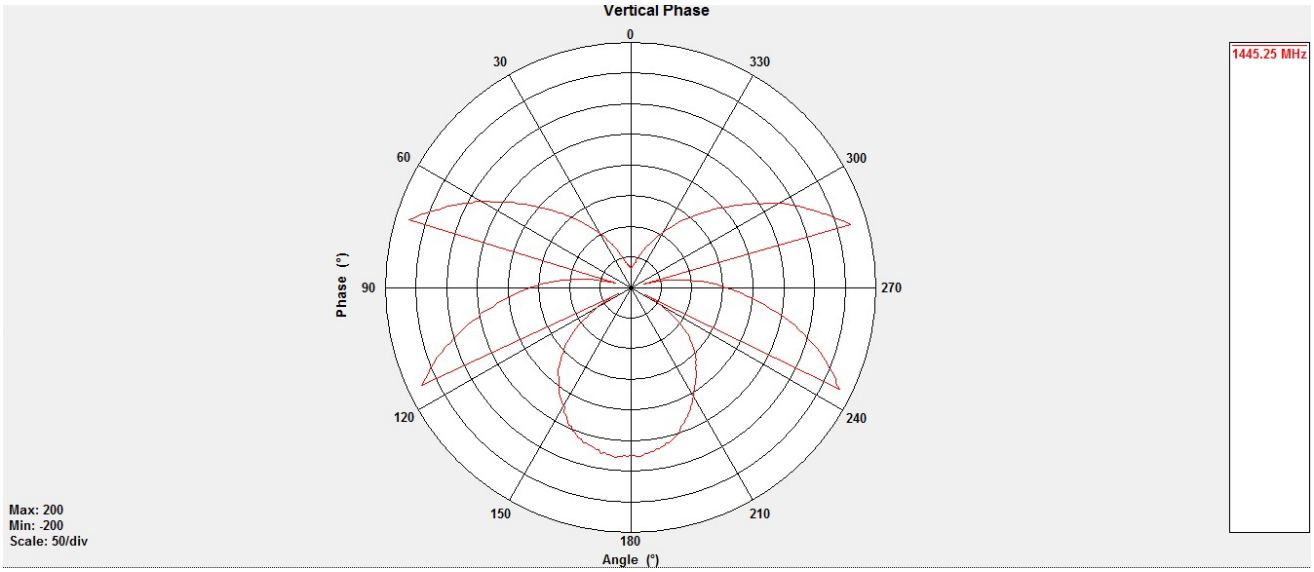

Fig. 5.9: Azimuthal phase pattern for element 1.

The gain and phase patterns for element 2 are given in polar plots for θ = 90° and 0° < Φ < 360° and a frequency of 1.44525 GHz in Figure 5.10 and Figure 5.11, respectively.

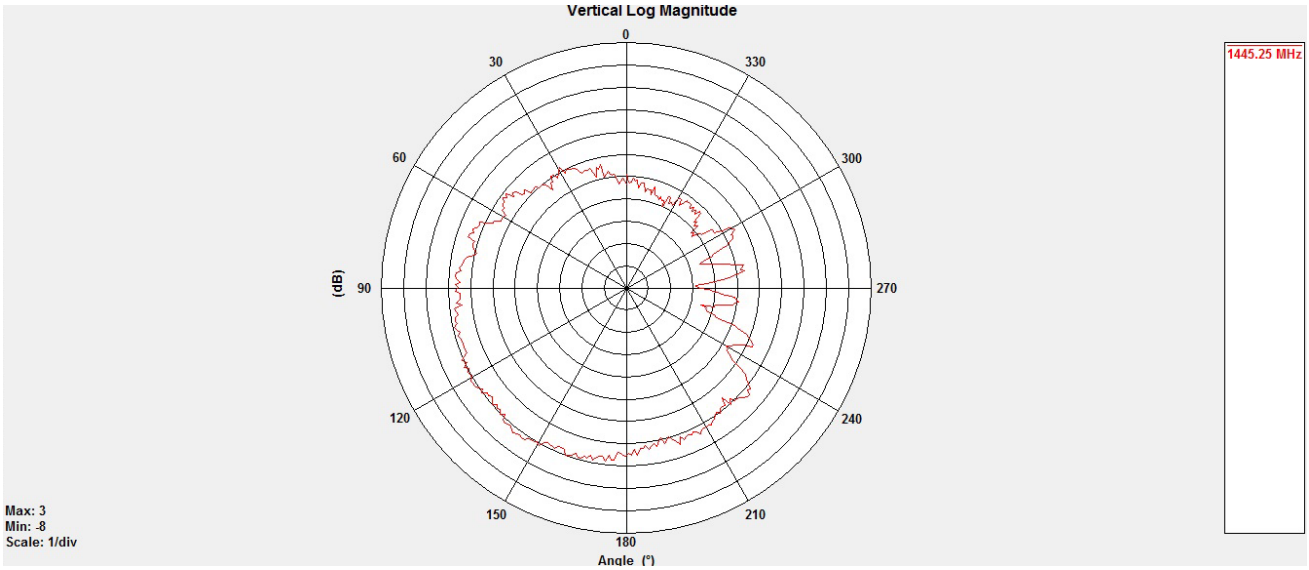

Fig. 5.10: Azimuthal gain radiation pattern for element 2.

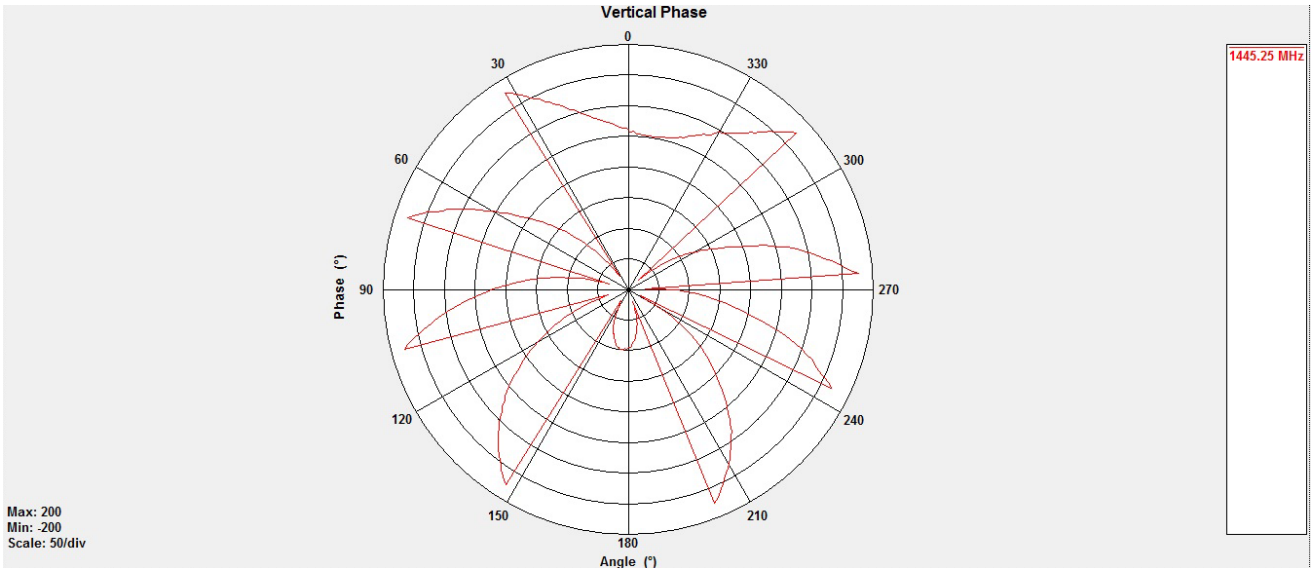

Fig. 5.11: Azimuthal phase pattern for element 2.

The gain and phase patterns for element 3 are given in polar plots for θ = 90° and 0° < Φ < 360° and a frequency of 1.44525 GHz in Figure 5.12 and Figure 5.13, respectively.

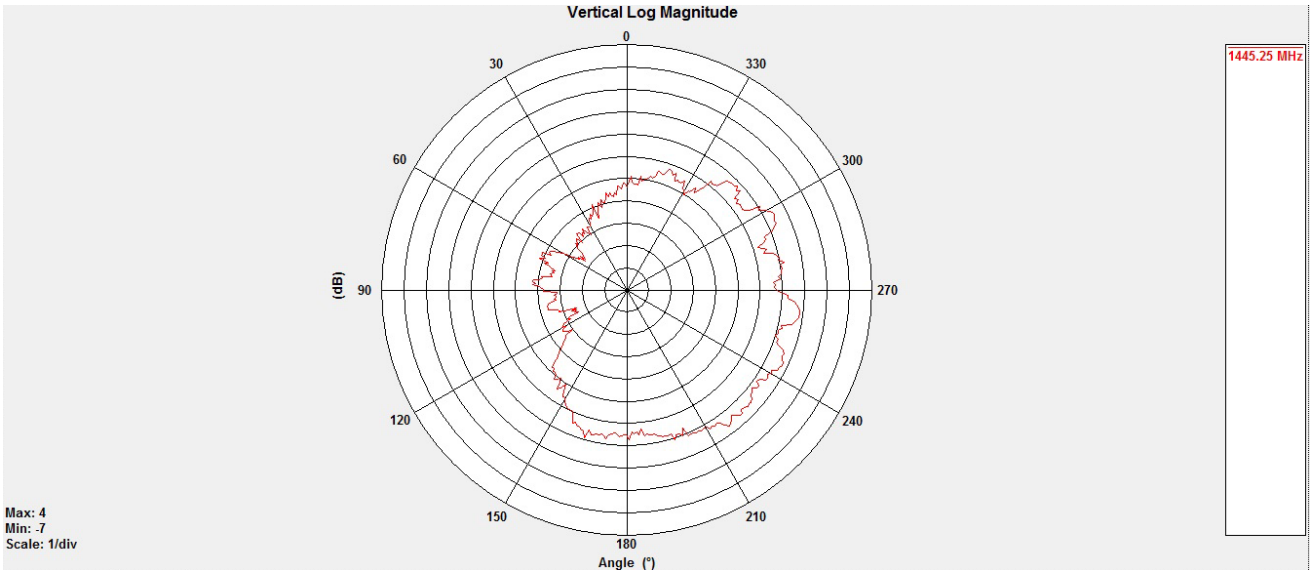

Fig. 5.12: Azimuthal gain radiation pattern for element 3.

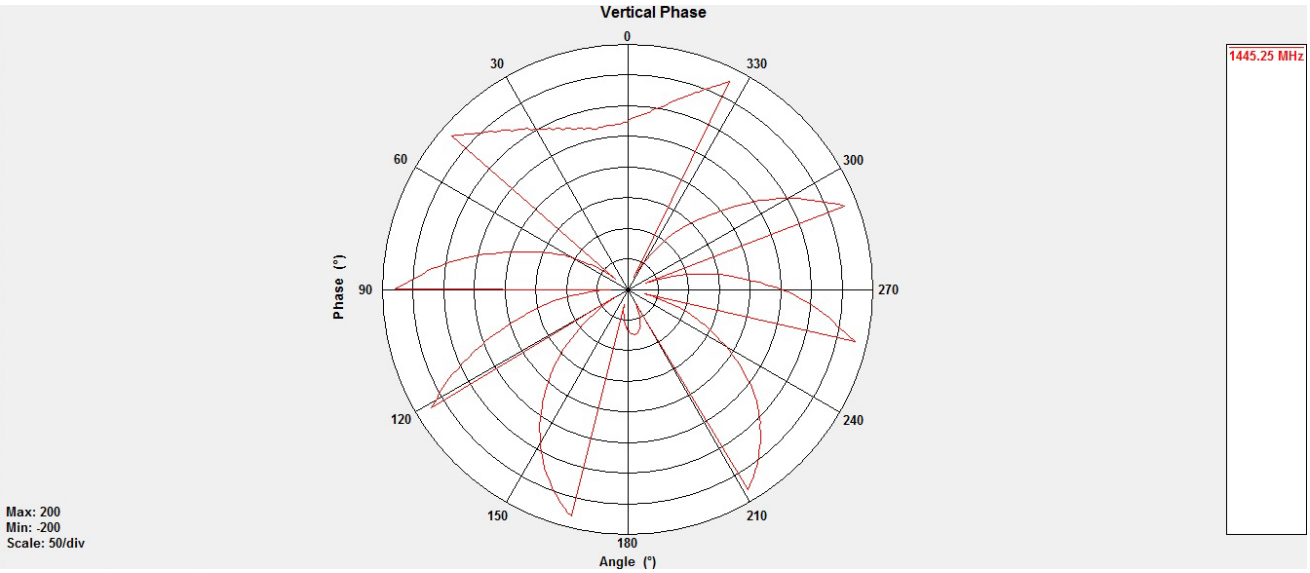

Fig. 5.13: Azimuthal phase pattern for element 3.

The three elements have azimuthal radiation pattern shapes consistent with what was determined in HFSS^{TM}. The pattern has a higher gain at the azimuth angle where the antenna being tested is closer to (0° for element 1, 120° for element 2 and 240° for element 3). The azimuth angles where the other two elements (the ones terminated in 50 Ω loads) are closer to have the smallest gain since the element being excited sees a copper barrier at these two angles. Finally, the maximum gain for the three elements' azimuthal cuts is ~0 dB. Since there are losses and imperfections throughout the array, the maximum gain cannot be expected to reach its maximum value of ~ 4.8 dBi. These three aspects of the radiation pattern agree with the 3-D pattern, and the 2-D vertical and horizontal radiation pattern from HFSS^{TM}. This confirms that the antenna array is fully functional and agrees with the simulation results.

5.4 Assessment of Azimuth AoA Determination Based on Measured Results

The phase plots over the azimuth angles are useful to determine the azimuth AoA of an object approaching the radar. This was assessed in Chapter 1 of this report. Any object

approaching the radar is going to approach it at a specific azimuth AoA. For that AoA, each of the three elements has a phase value. The differences between any two of these phase values (δ_{12}, δ_{13} and δ_{23}) can be used to calculate the AoA. As explained in Chapter 1, if only one δ value was available, there would be an ambiguity in the azimuth location of the target, and that is why at least two δ values are required and three antenna elements are used.

Using Matlab®, the raw phase data from the three elements (presented graphically for a frequency of 1.44525 GHz in Figures 5.9, 5.11 and 5.13) is acquired from the .txt files generated using the EMQuest^{TM} Viewer available in the chamber. This data consists of 201 frequency points (between 1.35 and 1.5 GHz) and 361 angle values (from 0 to 360 degrees). After performing a text scan to scan the files for the phase data and saving the data for each element in individual matrices, the differences in phase (δ) between elements 1 and 2, 1 and 3, and 2 and 3 are calculated for all angles in all frequencies. Another matrix with wavelength values is generated so that equation 1.19 can be used to find the θ_{AB} values, where A and B are the two elements connected by the baseline being analyzed.

When the theta values are being calculated, a process called phase unwrapping needs to be done since some of the δ values are outside of the boundaries set by the argument of the inverse cosine in equation 1.19 (which accepts values between -1 and 1). Therefore, 2π needs to be added or subtracted to the delta values so that δ is between -180° and 180°. After phase unwrapping this data, θ_{21}, θ_{31}, and θ_{32} can be calculated for all frequencies and all angles values. These theta values for three different frequencies (1.35 GHz, 1.44525 GHz and 1.5 GHz) are shown in Figure 5.14 below. Note that at angles close to end-fire for that specific baseline, the theta values have a very high inaccuracy, as opposed to the high accuracy at angles close to broadside for the baseline in question.

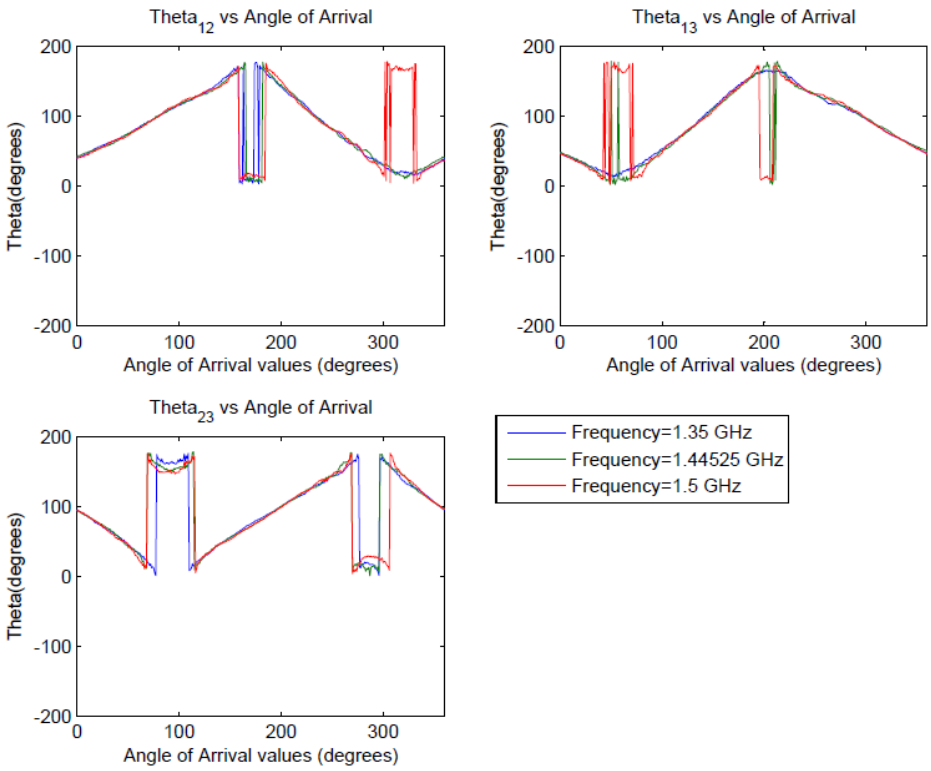

Fig. 5.14: Theta values vs. Theoretical AoAs for three different frequencies.

Since the baselines are not at the center of the array and are at 120° from each other, the theta values do not represent the actual target's AoA. A reference line needs to be chosen so that all theta values are given with respect to that reference line. Figure 5.15 shows this reference line and some important geometrical properties used in transforming the two theta options (as presented in Figure 1.4) into the two azimuth AoA possibilities for each baseline.

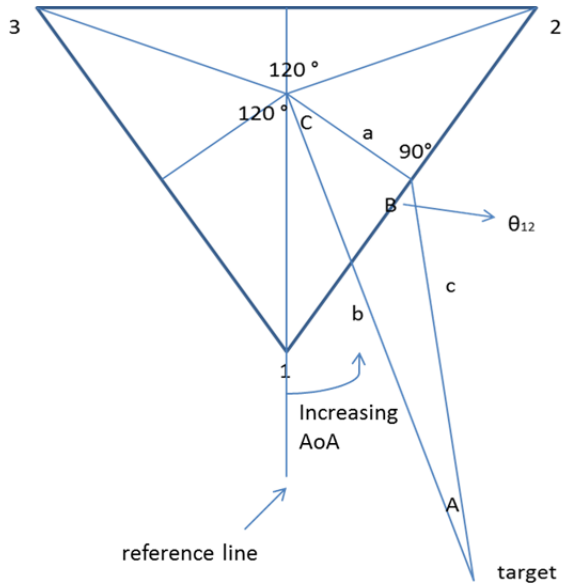

Fig. 5.15: Useful geometrical relationships used to determine AoA.

The most important equation used in determining the possible AoAs is the law of sines, shown in Equation 5.5 below [27].

$$\frac{\sin A}{a} = \frac{\sin B}{b} = \frac{\sin C}{c}$$

where A, B, C, a, b and c are shown in Figure 5.15.

The final step in determining the correct AoA out of the two possibilities is to remove the ambiguity present in the calculations. To do this, the two possible AoAs for each baseline are analyzed. These two possibilities for two different frequencies (1.35 GHz and 1.5 GHz) for the three baselines are shown in Figure 5.16 below. Note, again, that at angles close to end-fire for that specific baseline, the possible AoA values have a very high inaccuracy, as opposed to the high accuracy at angles close to broadside for the baseline in question.

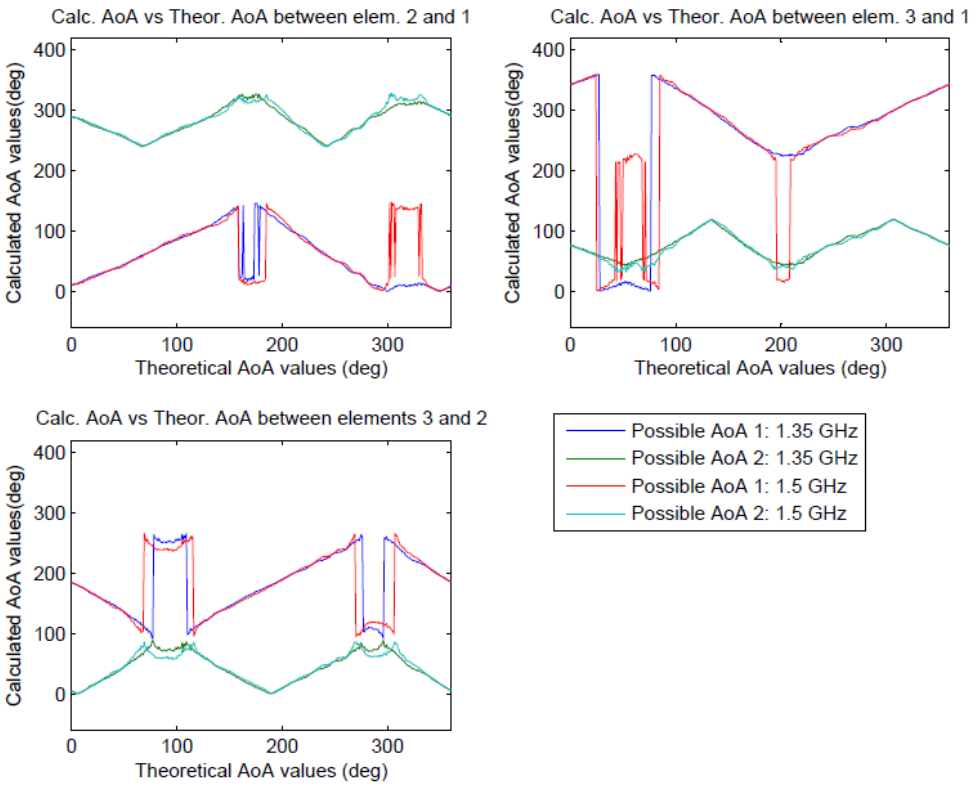

Fig. 5.16: Two possible AoA values vs. Theoretical AoAs for two different frequencies.

From these plots, it is possible to decide which of the two possibilities for each baseline is the one closer to the theoretical AoA values. So, for the angles where the curve has a good accuracy, these plots enable the correct choice between the two curves.

Finally, averaging is done between the AoA_{31}, AoA_{21} and AoA_{32} values, as long as the AoA is far from the end-fire regions of AoA_{21} and AoA_{32} (making their data have a high uncertainty and be unsuitable for the averaging process). The AoA averaging is broken into regions at which a unique set of curves can be averaged. For example, from 0° to around 70°, possible AoA 1 between elements 2 and 1 and possible AoA 2 between elements 3 and 2 can be used in the averaging process. This averaging reduces the uncertainty in the AoA final value. This entire process is shown in the Matlab® code included in Appendix C. The final results for the determined AoA are shown in Figure 5.17 below.

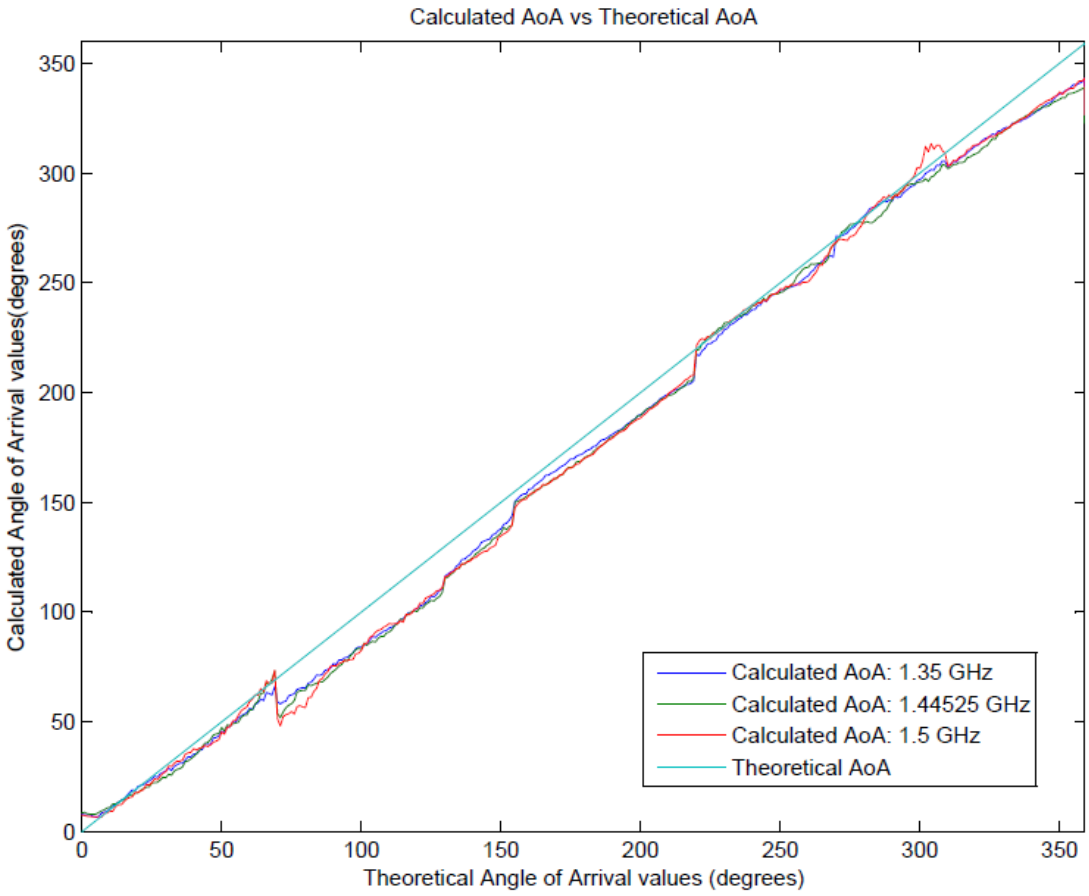

Fig. 5.17: Final calculated AoA values vs. Theoretical AoAs for three different frequencies.

Notice that at AoAs between 0° and ~70° and between ~220° to ~300° the calculated AoA is very accurate and, therefore, close to the theoretical AoA curve. At certain points the calculated AoA matches the theoretical AoA almost exactly. For AoAs between ~70° and ~220° and between ~300° and 360°, the calculated AoA is not as accurate as in the other two angle ranges. At these ranges, the calculated AoA is always smaller than the theoretical value, but it is never smaller than ~20° from the theoretical curve. This means that if ~5° to ~10° was added to the calculated values, the calculated curves would have a better match to the theoretical values. Figure 5.18 shows the error in the calculated AoA vs. the theoretical AoA (assuming that positive values in the error mean that the calculated AoA is less than the theoretical AoA) at the center

frequency. It also shows the mean for the error in the calculated AoA and the standard deviation.

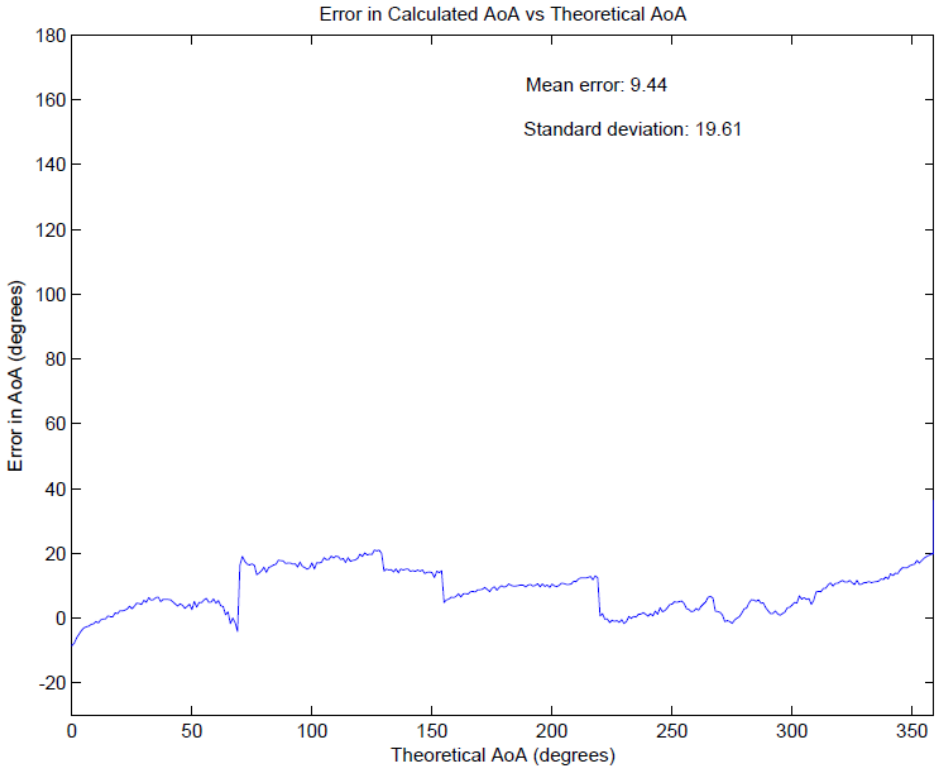

Fig. 5.18: Error in calculated AoA values vs. Theoretical AoAs at 1.44525 GHz.

Notice that the mean error is +9.44°, which means that the calculated AoA has a bias. If 9.44° is added to all the calculated values, the bias is removed and the maximum and minimum error values get reduced to under ±10°. This is still above the ±3° accuracy that was set as a goal, but with a better averaging process, this error might be reduced. The calculated values for the AoA with the removed bias are shown in Figure. 5.19.

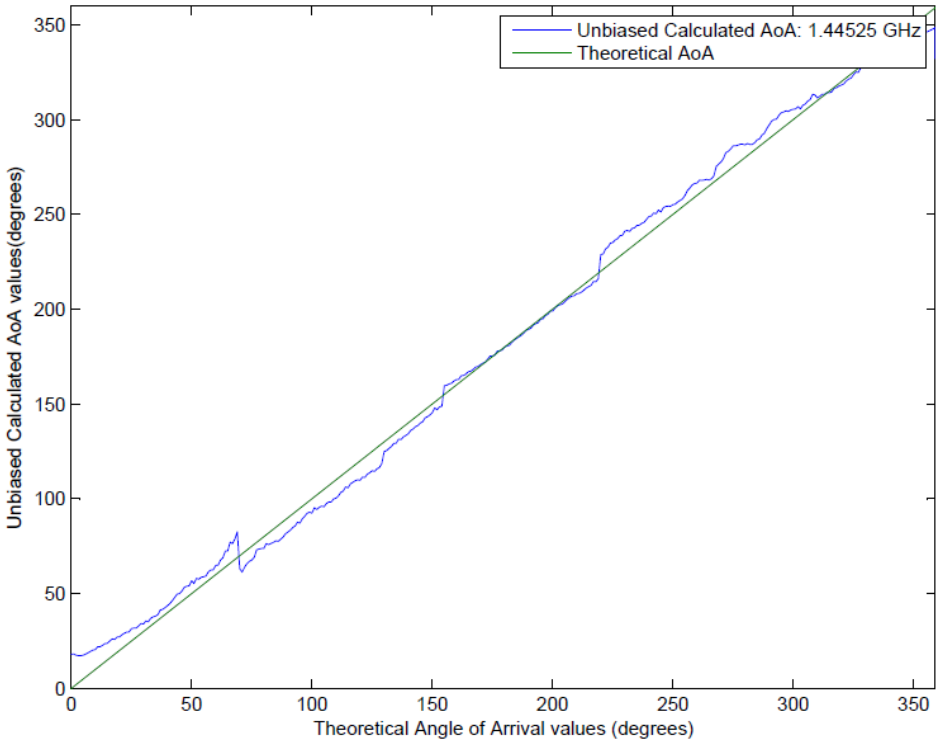

Fig. 5.19: Unbiased calculated AoA values vs. Theoretical AoAs at 1.44525 GHz.

6.1 Conclusion

The antenna array is fully functional and all the parameters tested match the simulation results. All its elements have good reflection coefficients and coupling parameters (below -10 dB) for a frequency range from 1.35 to 1.5 GHz. Each reflection coefficient and coupling curve is very close to the other curves of the same parameter, meaning that the elements are identical and have the right spacing between them. Since this array is used for azimuthal AoA measurements, the azimuthal radiation patterns (for $\theta = 90°$) are analyzed for the three elements. The gain magnitude patterns have a maximum of ~0 dBi at the azimuth angles where the element analyzed is closer to. This is also very close to the simulation results. Finally, in accordance with theory, the phase patterns over azimuthal angles are symmetrical, therefore the need for three antenna elements to eliminate an ambiguity in the AoA. When calculating the AoA, the results show that the theoretical and calculated results have a fairly good match (not ideal) and these two values diverge by at most ±10° after the bias has been removed.

The ABS plastic dome design was also successful. It is a material that provides protection for the array, with a weight that is not too heavy and barely any attenuation in the array's radiation pattern (~ 1 dB at most) even at a very small separation of less than 3 cm. Therefore, this material proved to be a good alternative when used as a protective structure for antenna arrays.

6.2 Future Work

In order to be used in smaller UAVs, the dimensions of the array need to be reduced. Both the elements and the ground plane need to be smaller. The best way to be able to decrease the

array dimensions is to increase the frequency used. The higher frequency bands that could be used according to the FCC allocation table [26] are two: from 2.4 GHz to 2.5 GHz and from 5.725 GHz to 5.875 GHz. The array could be made significantly smaller at the frequency band centered at 5.8 GHz. This would be its most clear advantage over the band centered at 2.45 GHz. Still, there might be some advantages in using the band centered at 2.45 GHz including lower s parameter levels, complexity and weight of the other components forming the radar. Therefore, the advantages of one band over the other could be further investigated.

Appendix A:

Comparison of Simulation and Theoretical Values of s_{21} Between Transmitter and Receiver Antennas

Assumptions									
Two antennas (trasnmitter and receiver) are polarization matched					Wavelength (m)				
Connected to matched t-lines					0.207555				
quarter-wave monopole Gain = 3.27 = 5.15 dBi									
Ptx = 1 W									
Equations used [24]				**Frequency (GHz)**	**Tx Placement (m, m, m)**	**Excitation 1**	**Excitation 2**	**|s21| (dB)**	**R(m)**	**Theor. |s21| (dB)**
				1.4454	(0,2,0)	Tx	Rx 1	-36	2.2008	-32.20
$\frac{P_r}{P_t} = G_t G_r \left(\frac{\lambda}{4\pi R}\right)^2$				1.4454	(0,2,0)	Tx	Rx 2	-33.2	1.9502	-31.15
				1.4454	(0,2,0)	Tx	Rx 3	-36.8	2.064	-31.64
				1.4454	(2,0,0)	Tx	Rx 1	-32.2	1.9423	-31.12
$Insertion\ Loss = 10log\frac{P_t}{P_r}$				1.4454	(2,0,0)	Tx	Rx 2	-37.5	2.0295	-31.50
				1.4454	(2,0,0)	Tx	Rx 3	-37.6	2.0295	-31.50
				1.4454	(0,-2,0)	Tx	Rx 1	-36.1	2.0008	-31.37
$Insertion\ Loss = -20\log\lvert s_{21}\rvert$				1.4454	(0,-2,0)	Tx	Rx 2	-36.7	2.064	-31.64
				1.4454	(0,-2,0)	Tx	Rx 3	-33.2	1.9502	-31.15
$s_{21}(dB) = 20\log\lvert s_{21}\rvert$				1.4454	(-2,0,0)	Tx	Rx 1	-36.1	2.0577	-31.62
				1.4454	(-2,0,0)	Tx	Rx 2	-33.9	1.9717	-31.25
				1.4454	(-2,0,0)	Tx	Rx 3	-46.9	1.9717	-31.25

Table 12 Electrical properties of thermoplastic materials

Property	ASTM method	Acetal	ABS	Acrylic	Cellulose acetate	Cellulose acetate butyrate	Cellulose propionate	Chlorinated polyether	Chlorotrifluoroethylene	Nylon (polyamide)	Polycarbonate
Arc resistance	D 495	129	90	No track	200	...	180	...	>360	140	120
Dielectric constant											
At 60 Hz	D 150	3.8	3.0	4.0	7.5	6.4	4.0	3.1	2.8	5.5	3.2
At 1 MHz		3.8	3.0	3.5	7.0	6.3	4.0	3.0	2.7	4.9	3.0
At 1 GHz	...	3.8	3.0	3.2	7.0	6.2	3.6	2.9	2.5	4.7	3.0
Dissipation factor											
At 60 Hz	D 150	0.004	0.003	0.04	0.01	0.02	0.01	0.01	0.001	0.01	0.0009
At 1 GHz	...	0.004	0.005	0.02	0.01	0.05	0.01	0.01	0.09	0.03	0.01
Dielectric strength, step-by-step, MV/m (V/mil)	D 149	16 (400)	14 (350)	14 (350)	8 (200)	10 (250)	12 (300)	16 (400)	18 (450)	12.8 (320)	14.5 (364)
Volume resistivity, Ω · m	D 257	10^{12}	10^{14}	10^{12}	10^{11}	10^{12}	10^{13}	10^{13}	10^{16}	10^{13}	10^{10}

Property	ASTM method	Polyethylene, low-density	Polyethylene, med-density	Polyethylene, high-density	Polypropylene	Polystyrene	Polysulfone	Polyphenylene oxide	Phenoxy	Polyvinyl chloride	Styrene-acrylonitrile	Tetrafluoro-ethylene
Arc resistance	D 495	140	200	200	185	100	122	75	...	80	150	<200
Dielectric constant												
At 60 Hz	D 150	2.4	2.4	2.4	2.6	3.4	3.1	2.6	4.1	3.6	3.4	2.1
At 1 MHz		2.4	2.4	2.4	2.6	3.2	3.1	2.6	4.1	3.3	2.5	2.1
At 1 GHz	...	2.4	2.4	2.4	2.6	3.1	3.1	2.6	3.8	3.4	3.1	2.1
Dissipation factor												
At 60 Hz	D 150	<0.0005	<0.0005	<0.0005	<0.0005	0.0004	0.0008	0.0004	0.001	0.007	0.004	<0.0002
At 1 MHz		<0.0005	<0.0005	<0.0005	<0.0005	0.0004	0.001	...	0.002	0.009	0.007	<0.0002
At 1 GHz	...	<0.0005	<0.0005	<0.0005	<0.0005	0.0004	0.005	0.0009	0.03	0.006	0.007	<0.0002
Dielectric strength, step-by-step, MV/m (V/mil)	D 149	16.8 (420)	20 (500)	22 (550)	18 (450)	12 (300)	16 (400)	16 (400)	16 (400)	15 (375)	12 (300)	17.2 (430)
Volume resistivity, Ω · m	D 257	10^{14}	10^{14}	10^{14}	10^{14}	10^{14}	10^{15}	10^{11}	10^{11}	10^{14}	10^{14}	10^{16}

Source: Ref 2

```
%azimuth_aoa_calc.m - Azimuth Angle of Arrival Calculation

%Author: Jose Florencio Neto
%Organization: University of Kansas
%Date: 2013-04-07
%Version: 1.0

%Clear screen.
clc

%Open text files.
fileID1 = fopen('Monopole_Array_Element_1.txt');

fileID2 = fopen('Monopole_Array_Element_2.txt');

fileID3 = fopen('Monopole_Array_Element_3.txt');

%Define N data points for data, frequency and angles.
N = 72561;

N_freq = 201;

N_angles = 361;

%Scan text for calculated phase for element 1 and store it in a matrix.
C_data1 = textscan(fileID1, '%d %f', N, 'delimiter', ',');

Data_elem_1=[C_data1{2}];

%Scan text for calculated phase for element 2 and store it in a matrix.
C_data2 = textscan(fileID2, '%d %f', N, 'delimiter', ',');

Data_elem_2=[C_data2{2}];

%Scan text for calculated phase for element 3 and store it in a matrix.
C_data3 = textscan(fileID3, '%d %f', N, 'delimiter', ',');

Data_elem_3=[C_data3{2}];

%Define speed of light.
c = 3*10^8;

%Frequency matrix preallocation.
Freq_values = zeros(N_freq,1);

%Create frequency matrix.
Initial_freq = 1350000000;
Freq_Increment = 750000;
for i=0:(N_freq-1)
    Freq_values(i+1,1) = Initial_freq + (Freq_Increment*i);
end
```

```
%Wavelength matrix preallocation.
lambda_values = zeros(N_freq,1);

%Create wavelength matrix.
for i=0:(N_freq-1)
    lambda_values(i+1,1) = c/Freq_values(i+1,1);
end

%Find delta between the phase of element 2 and element 1.
delta21 = degtorad(Data_elem_1) - degtorad(Data_elem_2);

%Find delta between the phase of element 3 and element 1.
delta31 = degtorad(Data_elem_1) - degtorad(Data_elem_3);

%Find delta between the phase of element 3 and element 2.
delta32 = degtorad(Data_elem_2) - degtorad(Data_elem_3);

%Theta between elements 2 and 1 matrix preallocation.
theta21_values = zeros(N_angles,N_freq);

%Create theta21 matrix.
for i=0:(N_freq-1)
    %Define the baseline value.
    baseline = lambda_values(i+1,1)/2;
    for j=0:(N_angles-1)
        %Perform phase unwrapping for deltas above acceptable domain.
        if (delta21((N_angles*i)+(j+1),1).*lambda_values(i+1,1)/(2*baseline*pi())) > 1
            delta21((N_angles*i)+(j+1),1) = delta21((N_angles*i)+(j+1),1)-(2*pi());

        %Perform phase unwrapping for deltas below acceptable domain.
        elseif (delta21((N_angles*i)+(j+1),1).*lambda_values(i+1,1)/(2*baseline*pi())) <↙
-1
            delta21((N_angles*i)+(j+1),1) = delta21((N_angles*i)+(j+1),1)+(2*pi());
        end

        %Calculate theta values.
        theta21_values(j+1,i+1) = radtodeg(acos(lambda_values(i+1,1).*delta21↙
((N_angles*i)+(j+1),1)./(2*pi()*baseline)));
    end
end

%Theta between elements 3 and 1 matrix preallocation.
theta31_values = zeros(N_angles,N_freq);

%Create theta31 matrix.
for i=0:(N_freq-1)
    %Define the baseline value.
    baseline = lambda_values(i+1,1)/2;
    for j=0:(N_angles-1)
        %Perform phase unwrapping for deltas above acceptable domain.
```

```
        if (delta31((N_angles*i)+(j+1),1).*lambda_values(i+1,1)/(2*baseline*pi())) > 1
            delta31((N_angles*i)+(j+1),1) = delta31((N_angles*i)+(j+1),1)-(2*pi());

        %Perform phase unwrapping for deltas below acceptable domain.
        elseif (delta31((N_angles*i)+(j+1),1).*lambda_values(i+1,1)/(2*baseline*pi())) <↙
-1
            delta31((N_angles*i)+(j+1),1) = delta31((N_angles*i)+(j+1),1)+(2*pi());
        end

        %Calculate theta values.
        theta31_values(j+1,i+1) = radtodeg(acos(lambda_values(i+1,1).*delta31↙
((N_angles*i)+(j+1),1)./(2*pi()*baseline)));
    end
end

%Theta between elements 3 and 1 matrix preallocation.
theta32_values = zeros(N_angles,N_freq);

%Create theta32 matrix.
for i=0:(N_freq-1)
    %Define the baseline value.
    baseline = lambda_values(i+1,1)/2;
    for j=0:(N_angles-1)
        %Perform phase unwrapping for deltas above acceptable domain.
        if (delta32((N_angles*i)+(j+1),1).*lambda_values(i+1,1)/(2*baseline*pi())) > 1
            delta32((N_angles*i)+(j+1),1) = delta32((N_angles*i)+(j+1),1)-(2*pi());

        %Perform phase unwrapping for deltas below acceptable domain.
        elseif (delta32((N_angles*i)+(j+1),1).*lambda_values(i+1,1)/(2*baseline*pi())) <↙
-1
            delta32((N_angles*i)+(j+1),1) = delta32((N_angles*i)+(j+1),1)+(2*pi());
        end

        %Calculate theta values.
        theta32_values(j+1,i+1) = radtodeg(acos(lambda_values(i+1,1).*delta32↙
((N_angles*i)+(j+1),1)./(2*pi()*baseline)));
    end
end

angles = 0:(N_angles-1);

%Plot theta12, theta13, and theta23 in the same figure vs theoretical angle of arrival.
%Label axes and assign legend to curves.
figure
subplot(221)
plot(angles, [theta21_values(1:N_angles,1),theta21_values(1:N_angles,128),theta21_values↙
(1:N_angles,201)]);
axis([0 360 -200 200]);
xlabel('Theoretical Angle of Arrival(degrees)');
ylabel('Theta(degrees)');
legend('Frequency=1.35 GHz','Frequency=1.44525 GHz','Frequency=1.5 GHz');
```

```
title('Theta_1_2 vs Angle of Arrival');

subplot(222)
plot(angles, [theta31_values(1:N_angles,1),theta31_values(1:N_angles,128),theta31_values
(1:N_angles,201)]);
axis([0 360 -200 200]);
xlabel('Theoretical Angle of Arrival(degrees)');
ylabel('Theta(degrees)');
legend('Frequency=1.35 GHz','Frequency=1.44525 GHz','Frequency=1.5 GHz');
title('Theta_1_3 vs Angle of Arrival');

subplot(223)
plot(angles, [theta32_values(1:N_angles,1),theta32_values(1:N_angles,128),theta32_values
(1:N_angles,201)]);
axis([0 360 -200 200]);
xlabel('Theoretical Angle of Arrival(degrees)');
ylabel('Theta(degrees)');
legend('Frequency=1.35 GHz','Frequency=1.44525 GHz','Frequency=1.5 GHz');
title('Theta_2_3 vs Angle of Arrival');

%Calculate azimuth AoA from theta21 and theta31.

%Define Range(m) from azimuth center to target.
range=5.7;

%Define distance from baseline center to azimuth center.
base_to_center=0.0306;

%Azimuth AoA option matrices preallocation.
option_1_azimuth_aoa21 = zeros(N_angles,N_freq);

option_2_azimuth_aoa21 = zeros(N_angles,N_freq);

option_1_azimuth_aoa31 = zeros(N_angles,N_freq);

option_2_azimuth_aoa31 = zeros(N_angles,N_freq);

option_1_azimuth_aoa32 = zeros(N_angles,N_freq);

option_2_azimuth_aoa32 = zeros(N_angles,N_freq);

%Create azimuth AoA matrix for theta between 1 and 2.
for i=0:(N_freq-1)
    for j=0:(N_angles-1)
        if (theta21_values(j+1,i+1) <= 90)
            %Find option 1 for AoA between elements 1 and 2.
            %Find 90 degree complement of theta value.
            option_1_theta21_complement = 90+theta21_values(j+1,i+1);

            %Use rule of sines to find angle between center of baseline and
            %azimuth center.
```

```
            option_1_angle_baseline_azcenter = asind(base_to_center*sind↙
(option_1_theta21_complement)/range);

            %Use triangle property to find azimuth AoA.
            option_1_angle_range_to_base_to_center = 180 -↙
option_1_angle_baseline_azcenter - option_1_theta21_complement;
            option_1_azimuth_aoa21(j+1,i+1) = abs(60 -↙
option_1_angle_range_to_base_to_center);

            %Find option 2 for AoA between elements 1 and 2.
            %Find 90 degree complement of theta value.
            option_2_theta21_complement = 90-theta21_values(j+1,i+1);

            %Use rule of sines to find angle between center of baseline and
            %azimuth center.
            option_2_angle_baseline_azcenter = asind(base_to_center*sind↙
(option_2_theta21_complement)/range);

            %Use triangle property to find azimuth AoA.
            option_2_angle_range_to_base_to_center = 180 -↙
option_2_angle_baseline_azcenter - option_2_theta21_complement;
            option_2_azimuth_aoa21(j+1,i+1) = abs(420 -↙
option_2_angle_range_to_base_to_center);
        else
            %Find option 1 for AoA between elements 1 and 2.
            %Find 90 degree complement of theta value.
            option_1_theta21_complement = 270-theta21_values(j+1,i+1);

            %Use rule of sines to find angle between center of baseline and
            %azimuth center.
            option_1_angle_baseline_azcenter = asind(base_to_center*sind↙
(option_1_theta21_complement)/range);

            %Use triangle property to find azimuth AoA.
            option_1_angle_range_to_base_to_center = 180 -↙
option_1_angle_baseline_azcenter - option_1_theta21_complement;
            option_1_azimuth_aoa21(j+1,i+1) = abs(60 +↙
option_1_angle_range_to_base_to_center);

            %Find option 2 for AoA between elements 1 and 2.
            %Find 90 degree complement of theta value.
            option_2_theta21_complement = 90-theta21_values(j+1,i+1);

            %Use rule of sines to find angle between center of baseline and
            %azimuth center.
            option_2_angle_baseline_azcenter = asind(base_to_center*sind↙
(option_2_theta21_complement)/range);

            %Use triangle property to find azimuth AoA.
            option_2_angle_range_to_base_to_center = 180 -↙
option_2_angle_baseline_azcenter - option_2_theta21_complement;
```

```
            option_2_azimuth_aoa21(j+1,i+1) = abs(60 +↙
option_2_angle_range_to_base_to_center);
        end
    end
end

%Create azimuth AoA matrix for theta between 1 and 3.
for i=0:(N_freq-1)
    for j=0:(N_angles-1)
        if (theta31_values(j+1,i+1) <= 90)
            %Find option 1 for AoA between elements 1 and 2.
            %Find 90 degree complement of theta value.
            option_1_theta31_complement = 90+theta31_values(j+1,i+1);

            %Use rule of sines to find angle between center of baseline and
            %azimuth center.
            option_1_angle_baseline_azcenter = asind(base_to_center*sind↙
(option_1_theta31_complement)/range);

            %Use triangle property to find azimuth AoA.
            option_1_angle_range_to_base_to_center = 180 -↙
option_1_angle_baseline_azcenter - option_1_theta31_complement;
            option_1_azimuth_aoa31(j+1,i+1) = abs(300 +↙
option_1_angle_range_to_base_to_center);

            %Bring angle measurement to the correct quadrant.
            if (option_1_azimuth_aoa31(j+1, i+1) > 360)
                option_1_azimuth_aoa31(j+1,i+1) = option_1_azimuth_aoa31(j+1,i+1) - 360;
            end

            %Find option 2 for AoA between elements 1 and 2.
            %Find 90 degree complement of theta value.
            option_2_theta31_complement = 90-theta31_values(j+1,i+1);

            %Use rule of sines to find angle between center of baseline and
            %azimuth center.
            option_2_angle_baseline_azcenter = asind(base_to_center*sind↙
(option_2_theta31_complement)/range);

            %Use triangle property to find azimuth AoA.
            option_2_angle_range_to_base_to_center = 180 -↙
option_2_angle_baseline_azcenter - option_2_theta31_complement;
            option_2_azimuth_aoa31(j+1,i+1) = abs(option_2_angle_range_to_base_to_center↙
- 60);
        else
            %Find option 1 for AoA between elements 1 and 2.
            %Find 90 degree complement of theta value.
            option_1_theta31_complement = 270 - theta31_values(j+1,i+1);

            %Use rule of sines to find angle between center of baseline and
            %azimuth center.
```

```
            option_1_angle_baseline_azcenter = asind(base_to_center*sind↙
(option_1_theta31_complement)/range);

            %Use triangle property to find azimuth AoA.
            option_1_angle_range_to_base_to_center = 180 -↙
option_1_angle_baseline_azcenter - option_1_theta31_complement;
            option_1_azimuth_aoa31(j+1,i+1) = abs(300 -↙
option_1_angle_range_to_base_to_center);

            %Bring angle measurement to the correct quadrant.
            if (option_1_azimuth_aoa31(j+1, i+1) > 360)
                option_1_azimuth_aoa31(j+1,i+1) = option_1_azimuth_aoa31(j+1,i+1) - 360;
            end

            %Find option 2 for AoA between elements 1 and 2.
            %Find 90 degree complement of theta value.
            option_2_theta31_complement = 90-theta31_values(j+1,i+1);

            %Use rule of sines to find angle between center of baseline and
            %azimuth center.
            option_2_angle_baseline_azcenter = asind(base_to_center*sind↙
(option_2_theta31_complement)/range);

            %Use triangle property to find azimuth AoA.
            option_2_angle_range_to_base_to_center = 180 -↙
option_2_angle_baseline_azcenter - option_2_theta31_complement;
            option_2_azimuth_aoa31(j+1,i+1) = abs(300 -↙
option_2_angle_range_to_base_to_center);
        end
    end
end

%Create azimuth AoA matrix for theta between 2 and 3.
for i=0:(N_freq-1)
    for j=0:(N_angles-1)
        if (theta32_values(j+1,i+1) <= 90)
            %Find option 1 for AoA between elements 1 and 2.
            %Find 90 degree complement of theta value.
            option_1_theta32_complement = 90+theta32_values(j+1,i+1);

            %Use rule of sines to find angle between center of baseline and
            %azimuth center.
            option_1_angle_baseline_azcenter = asind(base_to_center*sind↙
(option_1_theta32_complement)/range);

            %Use triangle property to find azimuth AoA.
            option_1_angle_range_to_base_to_center = 180 -↙
option_1_angle_baseline_azcenter - option_1_theta32_complement;
            option_1_azimuth_aoa32(j+1,i+1) = abs(180 -↙
option_1_angle_range_to_base_to_center);
```

```
            %Find option 2 for AoA between elements 1 and 2.
            %Find 90 degree complement of theta value.
            option_2_theta32_complement = 90-theta32_values(j+1,i+1);

            %Use rule of sines to find angle between center of baseline and
            %azimuth center.
            option_2_angle_baseline_azcenter = asind(base_to_center*sind↙
(option_2_theta32_complement)/range);

            %Use triangle property to find azimuth AoA.
            option_2_angle_range_to_base_to_center = 180 -↙
option_2_angle_baseline_azcenter - option_2_theta32_complement;
            option_2_azimuth_aoa32(j+1,i+1) = abs(180 -↙
option_2_angle_range_to_base_to_center);

            %Bring angle measurement to the correct quadrant.
            if (option_2_azimuth_aoa32(j+1, i+1) > 360)
                option_2_azimuth_aoa32(j+1,i+1) = option_2_azimuth_aoa32(j+1,i+1) - 360;
            end
        else
            %Find option 1 for AoA between elements 1 and 2.
            %Find 90 degree complement of theta value.
            option_1_theta32_complement = 270 - theta32_values(j+1,i+1);

            %Use rule of sines to find angle between center of baseline and
            %azimuth center.
            option_1_angle_baseline_azcenter = asind(base_to_center*sind↙
(option_1_theta32_complement)/range);

            %Use triangle property to find azimuth AoA.
            option_1_angle_range_to_base_to_center = 180 -↙
option_1_angle_baseline_azcenter - option_1_theta32_complement;
            option_1_azimuth_aoa32(j+1,i+1) = abs(180 +↙
option_1_angle_range_to_base_to_center);

            %Find option 2 for AoA between elements 1 and 2.
            %Find 90 degree complement of theta value.
            option_2_theta32_complement = 90-theta32_values(j+1,i+1);

            %Use rule of sines to find angle between center of baseline and
            %azimuth center.
            option_2_angle_baseline_azcenter = asind(base_to_center*sind↙
(option_2_theta32_complement)/range);

            %Use triangle property to find azimuth AoA.
            option_2_angle_range_to_base_to_center = 180 -↙
option_2_angle_baseline_azcenter - option_2_theta32_complement;
            option_2_azimuth_aoa32(j+1,i+1) = abs(180 +↙
option_2_angle_range_to_base_to_center);
```

```
            %Bring angle measurement to the correct quadrant.
            if (option_2_azimuth_aoa32(j+1, i+1) > 360)
                option_2_azimuth_aoa32(j+1,i+1) = option_2_azimuth_aoa32(j+1,i+1) - 360;
            end
        end
    end
end

%Azimuth AoA matrix preallocation.
azimuth_aoa = zeros(N_angles,N_freq);

%Compare azimuth AoA options to determine the actual azimuth AoA.
%Choose center frequency for determination between two theta31 options
%(since this theta has a smooth curve for all angles at this frequency).
Frequency = 128;

for i=0:(N_freq-1)
    for j=0:(N_angles-1)
        %Separate data into angle regions where calculated AoA matches
        %theoretical AoA.
        if (j < 70)
          %Perform averaging of good data to decrease error.
          azimuth_aoa(j+1,i+1) = (option_1_azimuth_aoa21(j+1,i+1) +↙
option_2_azimuth_aoa32(j+1,i+1))/2;

        elseif ((j >= 70) && (j < 130))
          %Perform averaging of good data to decrease error.
          azimuth_aoa(j+1,i+1) = (option_1_azimuth_aoa21(j+1,i+1) +↙
option_2_azimuth_aoa31(j+1,i+1))/2;

        elseif ((j >= 130) && (j < 155))
          %Perform averaging of good data to decrease error.
          azimuth_aoa(j+1,i+1) = (option_1_azimuth_aoa21(j+1,i+1) +↙
option_1_azimuth_aoa32(j+1,i+1))/2;

        elseif ((j >= 155) && (j < 220))
          azimuth_aoa(j+1,i+1) = option_1_azimuth_aoa32(j+1,i+1);

        elseif ((j >= 220) && (j < 270))
          %Perform averaging of good data to decrease error.
          azimuth_aoa(j+1,i+1) = (option_1_azimuth_aoa32(j+1,i+1) +↙
option_1_azimuth_aoa31(j+1,i+1))/2;

        elseif ((j >= 270) && (j < 310))
          %Perform averaging of good data to decrease error.
          azimuth_aoa(j+1,i+1) = (option_2_azimuth_aoa21(j+1,i+1) +↙
option_1_azimuth_aoa31(j+1,i+1))/2;

        elseif ((j >= 310) && (j < 360))
          azimuth_aoa(j+1,i+1) = option_1_azimuth_aoa31(j+1,i+1);
        end
```

```
    end
end

%Plot calculated AoA12, calculated AoA13 and calculated AoA23 in the same figure vs
theoretical angle of arrival.
%Label axes and assign legend to curves.
figure
subplot(221)
plot(angles, [option_1_azimuth_aoa21(1:N_angles,1), option_2_azimuth_aoa21(1:N_angles,1),
option_1_azimuth_aoa21(1:N_angles,201), option_2_azimuth_aoa21(1:N_angles,201)]);
axis([0 360 -60 420]);
xlabel('Theoretical AoA values (deg)');
ylabel('Calculated AoA values(deg)');
legend('Possible AoA 1: 1.35 GHz','Possible AoA 2: 1.35 GHz','Possible AoA 1: 1.5 GHz',
'Possible AoA 2: 1.5 GHz');
title('Calc. AoA vs Theor. AoA between elem. 2 and 1');

subplot(222)
plot(angles, [option_1_azimuth_aoa31(1:N_angles,1), option_2_azimuth_aoa31(1:N_angles,1),
option_1_azimuth_aoa31(1:N_angles,201), option_2_azimuth_aoa31(1:N_angles,201)]);
axis([0 360 -60 420]);
xlabel('Theoretical AoA values (deg)');
ylabel('Calculated AoA values(deg)');
legend('Possible AoA 1: 1.35 GHz','Possible AoA 2: 1.35 GHz','Possible AoA 1: 1.5 GHz',
'Possible AoA 2: 1.5 GHz');
title('Calc. AoA vs Theor. AoA between elem. 3 and 1');

subplot(223)
plot(angles, [option_1_azimuth_aoa32(1:N_angles,1), option_2_azimuth_aoa32(1:N_angles,1),
option_1_azimuth_aoa32(1:N_angles,201), option_2_azimuth_aoa32(1:N_angles,201)]);
axis([0 360 -60 420]);
xlabel('Theoretical AoA values (deg)');
ylabel('Calculated AoA values(deg)');
legend('Possible AoA 1: 1.35 GHz','Possible AoA 2: 1.35 GHz','Possible AoA 1: 1.5 GHz',
'Possible AoA 2: 1.5 GHz');
title('Calc. AoA vs Theor. AoA between elements 3 and 2');

%Theoretical angles preallocation.
theor_angles = zeros(N_angles,1);
%Create theoretical angle curve.
for j=0:(N_angles-1)
    theor_angles(j+1,1) = j;
end

%Plot calculated AoA vs theoretical AoA.
%Label axes and assign legend to curves.
figure
plot(angles, [azimuth_aoa(1:N_angles,1), azimuth_aoa(1:N_angles,128), azimuth_aoa(1:
N_angles,201), theor_angles(1:N_angles,1)]);
axis([0 359 0 360]);
xlabel('Theoretical Angle of Arrival values (degrees)');
```

```
ylabel('Calculated Angle of Arrival values(degrees)');
legend('Calculated AoA: 1.35 GHz','Calculated AoA: 1.44525 GHz','Calculated AoA: 1.5↙
GHz','Theoretical AoA');
title('Calculated AoA vs Theoretical AoA');

%Error values preallocation.
error = zeros(N_angles,1);
%Create error curve.
for j=0:(N_angles-1)
    %Use azimuth values at 1.44525 GHz.
    error(j+1,1) = j-azimuth_aoa(j+1,128);
end

%Calculate mean error.
mean_error = mean(error);

%Calculate standard deviation.
stdev_error = std(error);

%Plot error vs theoretical AoA.
%Label axes and assign legend to curves.
figure
plot(angles, error(1:N_angles,1));
axis([0 359 -30 180]);
xlabel('Theoretical AoA (degrees)');
ylabel('Error in AoA (degrees)');
gtext('Mean error: 9.44');
gtext('Standard deviation: 19.61');
title('Error in Calculated AoA vs Theoretical AoA');

%Unbiased AoA preallocation.
unbiased_azimuth_aoa = zeros(N_angles,1);
%Create error curve.
for j=0:(N_angles-1)
    %Use azimuth values at 1.44525 GHz.
    unbiased_azimuth_aoa(j+1,1) = azimuth_aoa(j+1,128) + mean_error;
end

%Plot unbiased calculated AoA vs theoretical AoA.
%Label axes and assign legend to curves.
figure
plot(angles, [unbiased_azimuth_aoa(1:N_angles,1), theor_angles(1:N_angles,1)]);
axis([0 359 0 360]);
xlabel('Theoretical Angle of Arrival values (degrees)');
ylabel('Unbiased Calculated AoA values(degrees)');
legend('Unbiased Calculated AoA: 1.44525 GHz','Theoretical AoA');

%Close text files.
fclose(fileID1);
```

```
fclose(fileID2);

fclose(fileID3);
```

[1] K.R. Demarest, *Engineering electromagnetics.*, Upper Saddle River: Prentice Hall, 1997, p. 414.

[2] K.R. Demarest, *Engineering electromagnetics.*, Upper Saddle River: Prentice Hall, 1997, p. 399.

[3] D.M. Pozar, *Microwave engineering.* 2nd ed., Hoboken: John Wiley & Sons Inc., 1998, p.198.

[4] D.M. Pozar, *Microwave engineering.* 2nd ed., Hoboken: John Wiley & Sons Inc., 1998, p.183.

[5] K.R. Demarest, *Engineering electromagnetics.*, Upper Saddle River: Prentice Hall, 1997, p. 403.

[6] K.R. Demarest, *Engineering electromagnetics.*, Upper Saddle River: Prentice Hall, 1997, p. 415.

[7] K.R. Demarest, *Engineering electromagnetics.*, Upper Saddle River: Prentice Hall, 1997, p. 587.

[8] K.R. Demarest, *Engineering electromagnetics.*, Upper Saddle River: Prentice Hall, 1997, pp. 594-596.

[9] G.W. Stimson, *Introduction to Airborne Radar.* 2nd ed., Raleigh: Scitech Publishing Inc., 2011, p. 7.

[10] C. Allen, "Radar measurements II," *EECS 725 Website*, p. 52, Dec. 2012. [Online]. Available: http://people.eecs.ku.edu/~callen/725/EECS725.htm. [Accessed Mar. 25, 2013].

[11] C. Allen, "Radar measurements I," *EECS 725 Website*, pp. 22-25, Dec. 2012. [Online]. Available: http://people.eecs.ku.edu/~callen/725/EECS725.htm. [Accessed Mar. 25, 2013].

[12] Personal Communication with Dr. Chris Allen

[13] G.W. Stimson, *Introduction to airborne radar.* 2nd ed., Raleigh: Scitech Publishing Inc., 2011, p. 473.

[14] V. Larson, "Radiation patterns," Jan. 2000. [Online]. Available: http://www.tscm.com/radiapat.pdf. [Accessed Mar. 25, 2013].

[15] S. Silver, *Microwave antenna theory and design.*, Stevenage: Peter Peregrinus Ltd, 1984, pp. 98-99.

[16] T. Macnamara, *Introduction to antenna placement and installation.*, Hoboken: John Wiley and Sons, 2010, p. 145.

[17] M.M. Khruslov, I.V. Ivanchenko & L.P. Lightart, "Size effect of the ground plane and axial coupling aperture on the monopole antenna performance," *2010 Int. Kharkov Symp. Physics Eng.*

Microwaves, Millimeter Submillimeter Waves (MSMW), June 2010.

[18] R. Bansal, "The far-field: How far is far enough?," *Applied Microwave & Wireless*, August 2006. [Online]. Available: http://people.eecs.ku.edu/~callen/725/Bansal1999AMWpp58.pdf. [Accessed Mar. 25, 2013].

[19] "Density values: selected resins," *Stelray Plastic Products, Inc.*, Oct. 2007. [Online]. Available: http://www.stelray.com/density_val.htm. [Accessed Mar. 25, 2013].

[20] C.A. Harper, *Handbook of plastic and elastomers.*, New York: McGraw-Hill, 1975, pp. 2-42.

[21] *Characterization and failure analysis of plastics.*, Materials Park: ASM International, 2003, p. 175.

[22] J.W. Nilsson, *Electric Circuits.*, Boston: Addison Wesley Longman Publishing Co, 1989, p. 95.

[23] "Scientific Atlanta 12-1.1," *Hitech-facility*, [Online]. Available: http://www.hitechfacility.co.jp/details.php?id=E0004107. [Accessed Mar. 25, 2013].

[24] C.A. Balanis, *Antenna theory: Analysis and design.* 3rd ed., Hoboken: Wiley-Interscience, 2005, p. 95.

[25] "How to Measure Antenna Gain(Part 1)-Gain Transfer Method," *Measurementest*, Sept.

2010. [Online]. Available: http://www.measurementest.com/2010/09/how-to-measure-antenna-gain-part-1-gain_08.html. [Accessed Mar. 25, 2013].

[26] "United States frequency allocations," *National Telecommunications & Inform. Administration*, Sept. 2011. [Online]. Available: http://www.ntia.doc.gov/files/ntia/publications/spectrum_wall_chart_aug2011.pdf. [Accessed Mar. 25, 2013].

[27] "Generalized Law of Sines," *Wolfram Mathworld*, Oct. 2002. [Online]. Available: http://140.177.205.23/GeneralizedLawofSines.html. [Accessed Mar. 25, 2013].